

COAL-LIKE SUBSTANCES FROM LOW-TEMPERATURE PYROLYSIS  
AT VERY LONG REACTION TIMESR. A. Friedel, J. A. Queiser, and H. L. RetcofskyU.S. Department of the Interior, Bureau of Mines,  
Pittsburgh Coal Research Center, Pittsburgh, Pa. 15213

## ABSTRACT

The importance of long reaction times in the coalification process has been demonstrated in the laboratory. Samples of cellulose and pine sawdust in evacuated, sealed glass vials have been heated at 200° C for two years. Black coal-like chars were produced; heating at 200° C for hours produced very little chemical change. The chars were characterized by infrared and electron spin resonance spectra. The infrared spectra of the pine sawdust char and of a subbituminous coal are nearly identical, except for differing carbonyl absorption. The spectrum of the cellulose char is also similar to that of the subbituminous coal. The electron spin resonance results show that g values and line widths are nearly identical for the chars and are very close to similar values for subbituminous coal.

200° C is considered a reasonable coalification temperature; depth of burial can provide such temperatures. The experimental coalification obtained in only two years appears to substantiate the hypothesis that geologic time could produce all ranks of coals at temperatures below 200° C.

## INTRODUCTION

In the study of the structure and properties of coal, attempts have been made to prepare synthetic coals, principally by pyrolysis methods. Chars having properties identical to those of coals have not been produced. Initial attempts at studying the infrared spectra of coal-like chars prepared by pyrolysis of pure materials were carried out several years ago.<sup>1,2/</sup> The pyrolysis method used was that of Smith and Howard, who had prepared from cellulose, chars that had some of the properties of coals.<sup>3/</sup> We studied the infrared spectra of chars prepared from cellulose over a range of temperatures; the spectrum of a 400° C cotton char somewhat resembled that of high-volatile bituminous coal.<sup>1,2/</sup> The spectrum of this char showed a definite carbonyl absorption band which is not present, except as a weak shoulder, in infrared spectra of coals. Carbohydrate chars prepared at 300°, 400°, and 500° C produced absorption bands in the aromatic region that were identical to the aromatic bands produced respectively by lignite, high-volatile bituminous, and anthracite coals; less similarity was observed in other parts of the spectra.<sup>4/</sup> Similarities of reaction of coal and the carbohydrate, sucrose, were nicely illustrated by the identical spectra of products obtained in hydrogenation studies.<sup>5/</sup>

Friedman and coworkers studied many coal-like chars prepared by pyrolysis of pure oxygenated compounds, mostly at 400° C and reaction times of one hour; several properties of these chars, including infrared spectra, have some resemblance to the corresponding properties of coals.<sup>6/</sup> Pure hydrocarbons have been charred in the presence and absence of molecular oxygen; only when oxygen was present did the infrared spectra of the chars resemble those of coals, particularly in the 1600 cm<sup>-1</sup> region.<sup>4,7/</sup> Unless oxygen is involved the 1600 cm<sup>-1</sup> band is weak or non-existent; thus it is believed that the strong 1600 cm<sup>-1</sup> band involves carbonyl groups.<sup>4,7/</sup>

In another study, chars were prepared from  $O^{18}$ -labelled compounds in an attempt to ascertain whether an isotopic shift would occur at  $1600\text{ cm}^{-1}$  and would thus indicate that carbonyl groups are involved. No isotopic shift was obtained; the infrared spectrum of an  $O^{18}$ -labelled chelate, dibenzoylmethane, demonstrated that if a C=O group is very strongly chelated the C=O vibration becomes completely delocalized and no isotopic shift occurs.<sup>8,9/</sup>

In attempting to simulate coal the following principal variables are available: Starting material, temperature, rate of heating, reaction time, and pressure. The effect of pressure is considered minor compared to the effect of temperature.<sup>10,11/</sup> The effect of pressure during many eons may be important; temperature during many eons is certainly important. Though presumptuous, it was assumed that some slight indication of the effect of geologic time might be observable in the laboratory. Pyrolysis experiments involving reaction times of years, rather than hours or days, were decided on. Temperatures at or below  $200^\circ\text{ C}$  were chosen. The spectral methods selected for investigation of the coal-like properties of the chars were infrared and electron spin resonance spectrometry.

#### EXPERIMENTAL PROCEDURE

Pyrolyses. Pyrolytic oxidation of cotton and pine-wood sawdust was carried out at low temperatures. Two sets of samples were heated in air at  $150^\circ\text{ C}$  and at  $200^\circ\text{ C}$  for 10 months; the chars produced were investigated by infrared spectrometry.

For the pyrolysis experiments without air, samples of cotton, 0.43 g, and pine-wood sawdust, 0.20 g, were placed in heavy-walled Pyrex tubes which were evacuated and sealed. The sample-tube volumes were 3.1 cc. The samples were heated at  $200^\circ\text{ C}$  for two years. Gases and other volatile products were analyzed by mass spectrometer.

Instrumental investigation. The principal methods of characterizing the pyrolysis products were infrared (Perkin-Elmer Model 521)<sup>a/</sup> and electron paramagnetic resonance spectrometry (Varian Associates Model V-4500). Preliminary examinations of the chars were also made on a high-resolution mass spectrometer (Consolidated 21-110B). Ultimate microanalyses of the chars will be performed by the Huffman Laboratories; analyses will destroy the small samples remaining so none will be carried out until all possible experimental investigations are concluded.

#### RESULTS AND DISCUSSION OF RESULTS

Low pyrolysis temperatures and reaction times of several months were decided on in an attempt to simulate mild coalification conditions. Temperatures in the  $200^\circ\text{ C}$  range are considered realistic; many coals have been subjected to such temperatures due to depth of burial. Initially pyrolytic oxidation runs were made on cellulose and on pine sawdust at  $150^\circ\text{ C}$  in the presence of air. Pyrolysis of these materials for 10 months gave black insoluble solids having infrared spectra which indicated extensive oxidation. The second set of investigations was carried out at  $200^\circ\text{ C}$  in the presence of air; as expected greater pyrolytic oxidation was produced. Then pyrolysis runs in the absence of air were initiated with samples of cotton and of pine sawdust sealed in evacuated, heavy-wall glass tubes. The samples were heated at  $200^\circ\text{ C}$  for two years. Tarry products were observed during the early stages of pyrolysis; these became solid char long before two years elapsed. The gas produced in the pyrolysis of the cotton sample was lost by an explosion; most of the char was salvaged. The vial containing the pine sawdust

<sup>a/</sup> Reference to trade names is made for identification only and does not imply endorsement by the Bureau of Mines.

char was then opened, with release of considerable pressure of gas (6.3 atm). A thin film of colorless liquid, mostly water, vaporized completely into the evacuated gas-handling system. The gas analysis in table 1 shows mainly H<sub>2</sub>O and CO<sub>2</sub>. Both chars were completely black; the yield of char from pine sawdust was about 85 percent. The infrared spectra of both samples are shown in figure 1, along with a spectrum of a subbituminous coal (Dietz bed, Wyoming, 70.8 percent C, m.a.f. Ultimate analysis is given in table 2). The spectra of the coal and the sawdust char are remarkably similar. In addition to the more obvious spectral similarities at 3400, 2950, 2920, 2860, 1600, 1440, 1370, 1280, and 1180 cm<sup>-1</sup>, there is a considerable similarity at the aromatic band positions, 860, 810, and 750 cm<sup>-1</sup>. The aromatic bands are weak in the spectra of subbituminous coals, but the similarity of the coal and char absorption patterns in this region is impressive. It is apparent from these spectra that it is possible over a long period of time to approach a coal-like spectrum, even at a low temperature.

Table 1.- Mass spectrometric analysis of gases from 200° pyrolysis of pine sawdust.  
Volume of vial, 3.1 cc; pressure in vial 6.3 atm.

	<u>Mole percent</u>	<u>Milligrams</u>
Carbon dioxide	25.8	9.7
Water	57.9	8.9
Methanol	3.9	1.1
Dimethyl ether	<u>12.4</u>	4.9
	100.	
Total carbonyl compounds (estimate)		<u>5.</u>
		29.6

Table 2.- Ultimate analysis of Dietz bed subbituminous coal,  
Big Horn Mine, Wyoming

	<u>Weight percent, m.a.f.<sup>a/</sup></u>
C	70.83
H	5.06
N	1.02
S	0.59
O (by difference)	22.50

a/ Ash content 3.23 percent (moisture-free)

Heating from room temperature to 190° C in one hour, the cellulose of Smith and Howard had produced a brown char (yield, 89 percent) but the infrared spectrum, as well as the elemental analysis, resembled those of cellulose with only minor differences.<sup>4/</sup> No coal-like spectral features were observed. In the spectrum of the sawdust char there is a 1700 band as we have seen before in char spectra. But, for the first time in spectra of chars prepared at low temperature the 1600 band is more intense than the 1700 and thus is approaching the situation in coal spectra. Thus the very long heating time has produced a definite decrease in carbonyl-containing structures. In the coalification process it is feasible that simple

carbonyl groups are first formed in the early stages of pyrolysis and then are slowly converted to some other structure(s) during geologic time. Possibly the carbonyl groups are converted to modified carbonyl structures which can produce the intense  $1600\text{ cm}^{-1}$  absorption band observed in infrared spectra of coals and chars. Substantiation of this hypothesis may exist in the behavior of carbonyl groups in chars that were prepared from cellulose at  $300^\circ$ ,  $400^\circ$ , and  $500^\circ\text{ C}$ .<sup>4,7/</sup> In the spectrum of the  $300^\circ$  char the carbonyl absorption is stronger than the unknown absorption at  $1600\text{ cm}^{-1}$ . Relative intensities are given in table 3. For the  $400^\circ\text{ C}$  char the intensities become more similar; the spectrum of the  $500^\circ\text{ C}$  char shows reversal of intensities with complete disappearance of the simple carbonyl absorption band.<sup>4,7/</sup> These changes may be explainable by the postulation of conversion into a modified carbonyl-containing structure. This structure could be the conjugated chelated structure, such as the enol form of acetylacetone, that has been proposed previously as the source of the  $1600\text{ cm}^{-1}$  absorption band.<sup>2,14/</sup> It is interesting that the same kind of change, though more subtle, occurs in coals; infrared spectra of lignites and low rank coals have weak absorption shoulders at  $1700\text{ cm}^{-1}$  which gradually disappear from spectra of higher rank coals.<sup>15,16/</sup> For the coals the conversion of carbonyl compounds to the presumed conjugated chelated carbonyls is farther advanced than it is in these chars which were prepared at reaction times of only one hour.<sup>4,7/</sup>

Table 3.- Relative absorption intensities in the infrared spectra of  $300^\circ$ ,  $400^\circ$ , and  $500^\circ\text{ C}$  cellulose chars at  $1700\text{ cm}^{-1}$  (carbonyl compounds) and  $1600\text{ cm}^{-1}$  (presumably chelated conjugated carbonyl groups)

<u>Cellulose char, preparation temperature</u>	<u>Relative intensities, percent</u>	
	<u><math>1700\text{ cm}^{-1}</math></u>	<u><math>1600\text{ cm}^{-1}</math></u>
$300^\circ\text{ C}$	78	22
$400^\circ\text{ C}$	59	41
$500^\circ\text{ C}$	0	100

Electron spin resonance spectrometry has been applied to the study of chars of cotton and pine sawdust. Values for the parameters are given in table 4 along with comparative values for subbituminous coal.<sup>17/</sup> As with the infrared, the results for the chars are closely similar to those for the coal vitrain. The fact that a signal is detected is of interest for it demonstrates that stable free radicals can be formed in natural materials on exposure to very mild heating conditions. There are not many examples of free radical signals obtained from chars produced at temperatures as low as  $200^\circ\text{ C}$ . It is probable that even lower temperatures will produce free radicals in carbonaceous materials over long periods of time.

Table 4.- Electron spin resonance data for chars and subbituminous coal vitrain

	<u>Cotton char</u>	<u>Pine sawdust char</u>	<u>Subbituminous vitrain, Wyoming</u>
g-Value	$2.00321 \pm 0.0001$	$2.00314 \pm 0.0001$	$2.00381 \pm 0.0001$
Line width, gauss	$5.6 \pm 0.5$	$6.3 \pm 0.5$	$8.0 \pm 0.5$

Preliminary work on mass spectra of these chars has shown mononuclear and polynuclear aromatics similar to those found in mass spectra obtained on coal; this investigation is continuing.

The striking importance of time in pyrolysis reactions has been demonstrated. If chars as coal-like as these can be produced in two years, at temperatures that have little effect during short times, then it appears that in geologic times coal could be produced at temperatures much lower than 200° as proposed by various people.<sup>10,12,13/</sup> Our next experiments will run for greater lengths of time, with the expectation of producing chars that will resemble higher ranks of coal. Under the same experimental conditions that produced chars similar to subbituminous coal, chars having the characteristics of bituminous coals possibly could result from heating at 200° C for three or four years. It is expected that the distinctive aromatic absorption bands in the infrared spectra and the electron spin resonance parameters, of bituminous coals will be duplicated in such chars.

On the question of whether cellulose or lignin is the more important precursor of coal the results herein described indicate that at low temperatures and long reaction times the coal-like chars obtained from cellulose and from lignin plus cellulose are very similar. It may be significant that greater similarity between coal and char infrared spectra is observed for the char from lignin plus cellulose (pine sawdust).

#### REFERENCES

1. Friedel, R. A., and Pelipetz, M. G., *J. Opt. Soc. Am.*, 1953, 43, 1051.
2. Friedel, R. A., and Queiser, J. A., *Anal. Chem.*, 1956, 28, 22.
3. Smith, R. C., and Howard, H. C., *J. Am. Chem. Soc.*, 1937, 59, 234.
4. Friedel, R. A., *Proc. Fourth Carbon Conf.*, Univ. Buffalo, Pergamon Press, New York, 1960, 321.
5. Pelipetz, M. G., and Friedel, R. A., *Fuel*, 1959, 38, 8.
6. Friedman, S., Raymond, R., Reggel, L., Wender, I., and Friedel, R. A., *Abstracts of Papers*, April 1956 meeting, *Am. Chem. Soc.*, 6J.
7. Friedel, R. A., *Applied Optics*, 1963, 2, 1109.
8. Friedel, R. A., Durie, R. A., and Shewchuk, Y., *Carbon*, 1967, 5, 559.
9. Durie, R. A., Shewchuk, Y., and Friedel, R. A., *Spectrochim. Acta*, 1968, 24A, 1543.
10. Teichmuller, M., and Teichmuller, R., Ch. in *Coal Science*, ed. R. F. Gould, *Advances in Chem. Series No. 55*, 1966, Washington, 133.
11. Hryckowian, E., Dutcher, R. R., and Dachille, F., *Econ. Geology*, 1967, 62, 517.
12. Karweil, J., *Deutsch Z. Geol. Ges.*, 1956, 107, 132.
13. Francis, W., *Coal*, E. Arnold Ltd., London, 1961, 573.

14. Brown, J. K., J. Chem. Soc., London, 1955, 744.
15. Friedel, R. A., Ch. in Applied Infrared Spectroscopy, ed. D. N. Kendall, Reinhold Pub. Co., 1966, 312.
16. Friedel, R. A., Retcofsky, H. L., and Queiser, J. A., Bureau of Mines Bull. 640, 1967, 48 pp.
17. Retcofsky, H. L., Stark, J. M., and Friedel, R. A., Anal. Chem., 1968, 40, 1699.

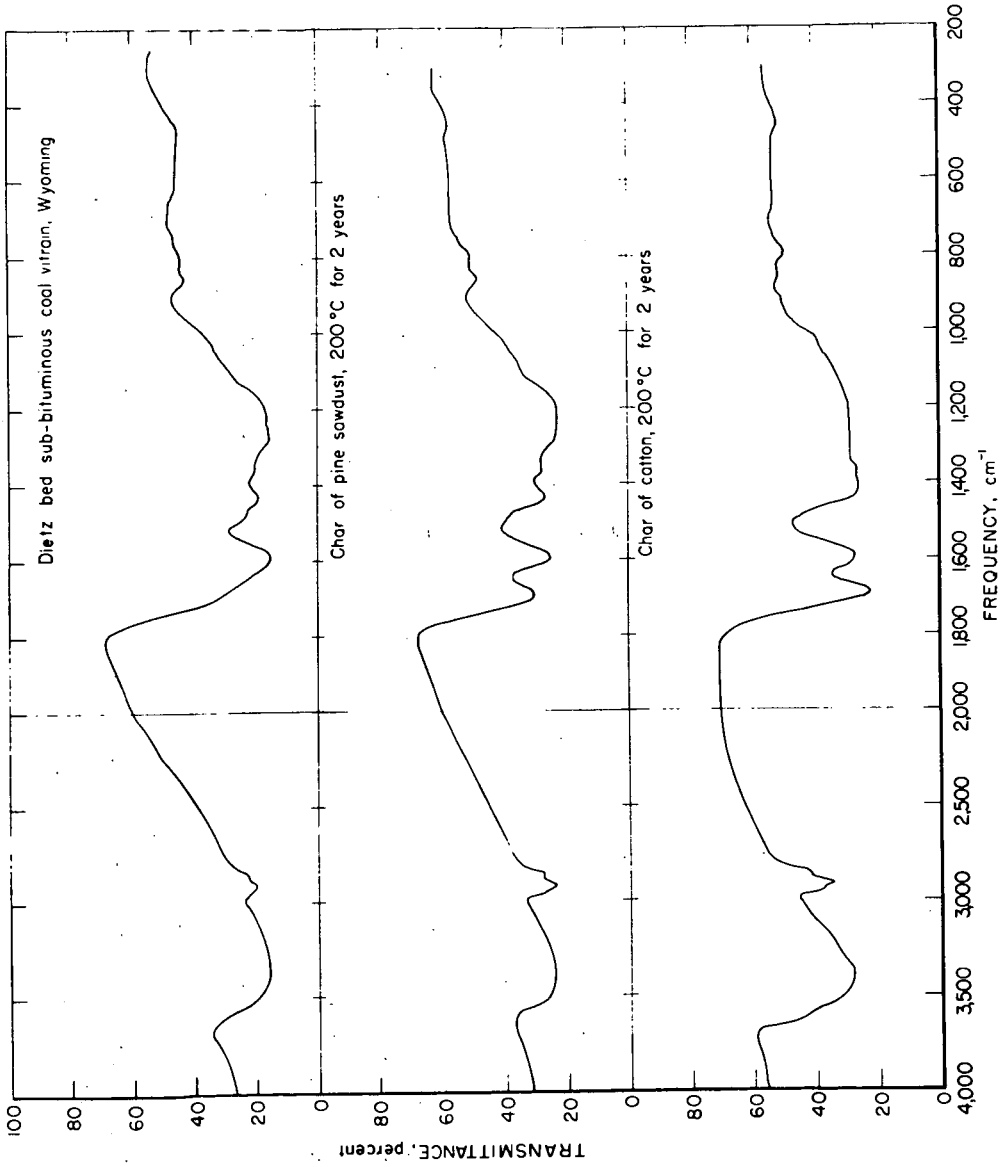


Figure 1.- Infrared spectra of Dietz bed subbituminous coal vitrain, 200° char of pine sawdust, and 200° char of cotton.

CHARACTERIZATION OF COAL LIQUEFACTION PRODUCTS BY  
HIGH RESOLUTION-LOW VOLTAGE MASS SPECTROMETRY

By

Thomas Aczel, J. Q. Foster, J. H. Karchmer  
Esso Research and Engineering Company, Baytown, Texas

## INTRODUCTION

High resolution mass spectroscopy is one of the most promising tools for the characterization of very complex materials. Since commercial instruments became available in the early nineteen sixties, the technique has been applied with considerable success to the analysis of materials derived both from petroleum and coal (1, 2, 3, 4).

This paper deals with the application of a particular approach, high resolution-low voltage mass spectrometry, coupled with computerized data acquisition and reduction, to the analysis of liquid and solid materials derived from coal liquefaction processes. These processes are of considerable industrial interest at the present; and the particular analytical approach used permits one to obtain routine quantitative or at least semiquantitative data on the hundreds of components present in each sample. Pilot plant or bench scale experiments can be thus supported with detailed analytical data.

## EXPERIMENTAL

The high resolution-low voltage technique used, as well as the computerized data acquisition and reduction system, has been described elsewhere (5, 6, 7). In brief, mass spectra are obtained on an AEI model MS 9 instrument at a resolving power of approximately 1/10,000, and at low ionizing voltages, approximately 12 volts. This resolving power is sufficient to separate all significant mass multiplets up to about  $m/e$  400, with exception of the  $^{13}\text{CH-N}$  doublet, the separation of which requires additional calculations. At the same time, the use of low ionizing voltages reduces the spectra to essentially parent peaks and their  $^{13}\text{C}$  isotopes, so that interferences between sample components are practically eliminated, and data can be obtained both on the compound type and carbon number distribution. Quantitative information is obtained by using pure compound or extrapolated calibration coefficients. The data acquisition system consists of an IBM Model 1802 computer, which converts the analog signals from the mass spectrometer to digital data and records these on magnetic tape. Subsequent calculations, including the recognition of peaks, calculation of peak areas, precise masses, formulas and, finally, the complete quantitative analysis, are carried out on an IBM Model 360/50 computer. At present, the quantitative analysis provides data routinely for up to 58 compound types and up to 2900 components, in less than three hours, including instrument time and interpretation. These types include hydrocarbons with formulas  $\text{C}_n\text{H}_{2n}$  to  $\text{C}_n\text{H}_{2n-44}$ , oxygenated compounds from  $\text{C}_n\text{H}_{2n-20}$  to  $\text{C}_n\text{H}_{2n-36}\text{O}$ , and sulfur compounds from  $\text{C}_n\text{H}_{2n-2}\text{S}$  to  $\text{C}_n\text{H}_{2n-34}\text{S}$ . Semiquantitative information on additional compound types, such as those containing N, or containing more than one heteroatom per molecule, or possessing a higher condensation than outlined above, can be obtained in a short additional time. The analysis is normalized to the volatile portion of each sample, determined by weighing the sample and any observed residue.

## DISCUSSION

Application of the high resolution-low voltage method to coal liquefaction products yields a very detailed characterization. Isomeric hydrocarbon types, possessing the same general formula, but different aromatic nuclei, can be separated and determined at least semiquantitatively. The behavior of the components during processing can be closely followed. The analysis includes data on aromatic and heteroaromatic components ranging from ppm to several percent in concentration and from 78 to 500+ in molecular weight. A large number of components and compound types can be determined rapidly in each sample. The degree of sophistication attained is best illustrated with practical examples.

The ability of distinguishing isomeric hydrocarbon types is based on the observed fact that the concentrations of the aromatic nuclei are higher than those of the alkyl-substituted members in any homologous series. Thus maxima in the carbon number distribution in any series correspond in most cases to the appearance of an individual nucleus. A number of these nuclei are naphthenoaromatic compounds. Examination of samples hydrogenated to different extents can thus corroborate the presence of naphthenoaromatic nuclei, as the concentration of these increases with the extent of the hydrogenation. The data reported below will serve to illustrate the procedure.

Carbon Number Distribution in the  $C_nH_{2n-10}$  Series, Weight Percent

<u>Formula</u>	<u>Mildly Hydrogenated Material</u>	<u>Severely Hydrogenated Material</u>
$C_9H_8$	0.062	0.056
$C_{10}H_{10}$	0.220	0.408
$C_{11}H_{12}$	0.168	0.162
$C_{12}H_{14}$	0.444	0.926
$C_{13}H_{16}$	0.552	1.175
$C_{14}H_{18}$	0.702	1.493
$C_{15}H_{20}$	0.278	0.624
$C_{16}H_{22}$	0.314	0.443
$C_{17}H_{24}$	0.122	0.252
$C_{18}H_{26}$	0.006	0.088

The only reasonable structure for a  $C_9H_8$  hydrocarbon is indene.  $C_{10}H_{10}$  could be methyl-indene or dihydronaphthalene. As the total  $C_{10}$  concentration is higher than the  $C_9$  concentration, dihydronaphthalene is believed to be the major component. This assumption is corroborated by the fact that this difference in concentration is enhanced in the more severely hydrogenated material, and dihydronaphthalene is an obvious hydrogenation product from naphthalene. Analogously, increases in concentration at  $C_{12}$ ,  $C_{13}$ ,  $C_{14}$ , and  $C_{16}$ , all enhanced in the severely hydrogenated material, indicate the presence of additional nuclei, respectively identified as tetrahydroacenaphthene, benzohydrindane, octahydroanthracene and dodecahydropyrene. Data from other series of the same general formula are treated similarly. Only maxima or increases in concentration which appear at the same carbon number and series in a large number of samples are accepted as a genuine indication of more than one compound type in a given series.

As mentioned above, the concentration of alkyl-substituted components is considerably lower than that of the respective nuclei. This can be observed best in series and carbon number intervals where only one compound type is present, as shown below.

Carbon Number Distribution in the  $C_nH_{2n-8}$  Series, Weight Percent

<u>Formula</u>	<u>Mildly Hydrogenated Material</u>	<u>Severely Hydrogenated Material</u>
$C_{10}H_{12}$	5.804	9.180
$C_{11}H_{14}$	2.977	5.291
$C_{12}H_{16}$	1.805	2.671
$C_{13}H_{18}$	1.043	1.291

The decrease in concentration with increasing carbon number is approximately twofold. This rate of decrease has also been observed for other series, and in a large number of samples. We were able thus to develop a method to estimate the concentration of each isomeric compound type in a given series. The procedure, illustrated below, starts with extrapolating the concentrations of the homologs of the compound type with the lowest molecular weight nucleus. The concentration of the nucleus of the next compound type is obtained by subtracting the extrapolated concentration of the homolog of the first compound type at the carbon number involved from the concentration observed for the series. Concentrations of the homologs of the second compound type are then extrapolated; and the procedure continues similarly for all other compound types. The extrapolation is used, of course, only in carbon number intervals where more than one type is conceivably present. In addition, the method is applicable only to samples with boiling range wide enough to contain all isomers involved in the separation.

Separation of Isomeric Compound Types in the  $C_nH_{2n-14}$  Series, Weight Percent

<u>Formula</u>	<u>Total <math>C_nH_{2n-14}</math> Series</u>	<u>Acenaphthenes</u>	<u>Tetrahydro-anthracenes</u>	<u>Octahydro-pyrenes</u>
$C_{12}H_{10}$	2.954 <sup>(1,2)</sup>	2.954 <sup>(2)</sup>	-	-
$C_{13}H_{12}$	1.894 <sup>(2)</sup>	1.894 <sup>(2)</sup>	-	-
$C_{14}H_{14}$	2.536 <sup>(1,2)</sup>	0.947 <sup>(3)</sup>	1.589 <sup>(4)</sup>	-
$C_{14}H_{16}$	1.105 <sup>(2)</sup>	0.474 <sup>(3)</sup>	0.631 <sup>(4)</sup>	-
$C_{16}H_{18}$	1.146 <sup>(1)</sup>	0.237 <sup>(3)</sup>	0.316 <sup>(3)</sup>	0.593 <sup>(4)</sup>
$C_{17}H_{20}$	0.631 <sup>(2)</sup>	0.118 <sup>(3)</sup>	0.158 <sup>(3)</sup>	0.355 <sup>(4)</sup>
$C_{18}H_{22}$	0.316 <sup>(2)</sup>	0.059 <sup>(3)</sup>	0.079 <sup>(3)</sup>	0.178 <sup>(4)</sup>

- (1) Maxima in carbon number distribution, indicating the appearance of respectively, acenaphthene, tetrahydroanthracene and octahydro-pyrene.
- (2) Raw concentrations.
- (3) Concentrations obtained by extrapolation.
- (4) Concentrations obtained by subtraction.

The information thus obtained on the concentration of the individual compound types can be used to follow their behavior upon hydrogenation. Typical data obtained are shown below.

Ring Systems	Weight Percent	
	Mildly Hydrogenated Material	Severely Hydrogenated Material
<u>Naphthalene System</u>		
Naphthalenes, $C_n H_{2n-12}$	14.2	7.9
Dihydronaphthalenes, $C_n H_{2n-10}$	0.5	0.7
Tetralins, $C_n H_{2n-8}$	11.5	18.4
Octahydronaphthalenes, $C_n H_{2n-4}$	0.3	0.4
Decalins, $C_n H_{2n-2}$	<u>2.0</u>	<u>2.6</u>
Total	28.5	30.0
<u>Anthracene System</u>		
Anthracenes, $C_n H_{2n-18}$	7.2	5.4
Tetrahydroanthracenes, $C_n H_{2n-14}$	3.0	3.8
Hexahydroanthracenes, $C_n H_{2n-12}$	1.3	1.5
Octahydroanthracenes, $C_n H_{2n-10}$	0.7	1.5
Decahydroanthracenes, $C_n H_{2n-8}$	<u>0.6</u>	<u>1.2</u>
Total	12.8	13.4
<u>Acenaphthene System</u>		
Acenaphthylenes, $C_n H_{2n-16}$	0.1	0.0
Acenaphthenes, $C_n H_{2n-14}$	6.6	5.3
Tetrahydroacenaphthenes, $C_n H_{2n-10}$	<u>0.7</u>	<u>1.7</u>
Total	7.4	7.0
<u>Fluorene System</u>		
Fluorenes	<u>5.0</u>	<u>5.0</u>
Total	5.0	5.0

Another aspect of the characterization of coal liquefaction products is the determination of components containing heteroatoms. Most of these can be directly identified from the computer output of the high resolution-low voltage spectra as illustrated below for typical mass multiplets.

Computer Identification of FormulasMultiplets at m/e 310 and 330

<u>Intensity, % I</u>	<u>Measured Mass</u>	<u>Error, mmu</u>	<u>Formula</u>
0.0016	310.0857	+0.7	C <sub>19</sub> H <sub>18</sub> S <sub>2</sub>
0.0332	310.1346	-1.2	C <sub>23</sub> H <sub>18</sub> <sup>0</sup>
0.5825	310.1736	+1.5	C <sub>24</sub> H <sub>22</sub>
0.0075	310.2276	-2.0	C <sub>22</sub> H <sub>30</sub> <sup>0</sup>
0.0435	310.2675	+1.5	C <sub>23</sub> H <sub>34</sub>
0.0017	330.1360	-4.8	C <sub>26</sub> H <sub>18</sub>
0.0064	330.1605	-1.5	C <sub>23</sub> H <sub>22</sub> O <sub>2</sub>
0.0131	330.1963	-2.1	C <sub>24</sub> H <sub>26</sub> <sup>0</sup>
0.1219	330.2360	+1.3	C <sub>25</sub> H <sub>30</sub>
0.0051	330.3291	+0.5	C <sub>24</sub> H <sub>42</sub>

The resolving power of our instrument, however, is insufficient to separate the <sup>13</sup>CH-N doublet above m/e 120-130. Components containing one N atom are therefore detected using isotope correction techniques. The presence of N compounds of odd molecular weights is indicated by residual peakheights after isotope correction and shift in the measured mass from the value of the <sup>13</sup>C isotope to that of the N compound, as shown in the example reported below.

<u>Measured Mass</u>	<u>Formula</u>	<u>Error, mmu</u>	<u>Intensity, % I</u>
180.093	C <sub>14</sub> H <sub>12</sub>	-0.6	1.903
181.090	-	-	0.845

<u>Formula</u>	<u>Theoretical Mass</u>	<u>Theoretical Intensity, % I</u>
<sup>13</sup> CC <sub>13</sub> H <sub>12</sub>	181.096	0.290
C <sub>13</sub> H <sub>11</sub> N	181.089	0.555*

• Residual after isotope correction.

Theoretical mass for unresolved doublet:

$$\frac{(181.096 \times 0.290) + (181.089 \times 0.555)}{0.845} = 181.091$$

Error of mass calculation for unresolved doublet: -1.0 mmu (-0.4 with respect to 180.093).

The techniques discussed above result in a thorough characterization of coal liquefaction products. The wealth of data obtained is illustrated by the list of compound types detected in one individual sample, reported below.

Series	Model Structure	Series	Model Structure
$C_n H_{2n}$	Cyclohexanes	$C_n H_{2n-20}$	Naphthenoanthracenes
$C_n H_{2n-2}$	Decalins	$C_n H_{2n-20}$	Tetrahydrochrysenes
$C_n H_{2n-2}$	Hydrindans	$C_n H_{2n-22}$	Pyrenes
$C_n H_{2n-4}$	Hydrindenes	$C_n H_{2n-22}$	Hexahydrobenzopyrenes
$C_n H_{2n-4}$	Octahydronaphthalenes	$C_n H_{2n-24}$	Chrysenes
$C_n H_{2n-4}$	Perhydroanthracenes	$C_n H_{2n-24}$	Tetrahydrobenzopyrenes
$C_n H_{2n-6}$	Benzenes	$C_n H_{2n-26}$	Cholanthrenes
$C_n H_{2n-8}$	Indanes	$C_n H_{2n-28}$	Benzopyrenes
$C_n H_{2n-8}$	Tetralins	$C_n H_{2n-30}$	Picenes
$C_n H_{2n-10}$	Indenes	$C_n H_{2n-32}$	Anthanthrenes
$C_n H_{2n-10}$	Dihydronaphthalenes	$C_n H_{2n-34}$	Dibenzopyrenes
$C_n H_{2n-10}$	Tetrahydroacenaphthenes	$C_n H_{2n-36}$	Coronenes
$C_n H_{2n-10}$	Benzhydrindanes	$C_n H_{2n-38}$	Benzanthanthrenes
$C_n H_{2n-10}$	Octahydroanthracenes	$C_n H_{2n-4}^S$	Thiophenes
$C_n H_{2n-10}$	Dodecahydropyrenes	$C_n H_{2n-10}^S$	Benzothiophenes
$C_n H_{2n-12}$	Naphthalenes	$C_n H_{2n-12}^S$	Naphthenobenzothiophenes
$C_n H_{2n-14}$	Acenaphthenes	$C_n H_{2n-14}^S$	Indenothiophenes
$C_n H_{2n-14}$	Tetrahydroanthracenes	$C_n H_{2n-16}^S$	Dibenzothiophenes
$C_n H_{2n-16}$	Acenaphthylenes	$C_n H_{2n-18}^S$	Acenaphthenothiophenes
$C_n H_{2n-16}$	Fluorenes	$C_n H_{2n-20}^S$	Fluorenothiophenes
$C_n H_{2n-16}$	Dihydroanthracenes	$C_n H_{2n-2}^O$	Dihydrofurans
$C_n H_{2n-16}$	Hexahydropyrenes	$C_n H_{2n-4}^O$	Furans
$C_n H_{2n-18}$	Anthracenes	$C_n H_{2n-6}^O$	Phenols
$C_n H_{2n-18}$	Tetrahydropyrenes	$C_n H_{2n-8}^O$	Naphthenophenols
$C_n H_{2n-18}$	Hexahydrochrysenes	$C_n H_{2n-10}^O$	Benzofurans
$C_n H_{2n-18}$	Decahydrobenzopyrenes	$C_n H_{2n-12}^O$	Naphthols
		$C_n H_{2n-14}^O$	Naphthenonaphthols
		$C_n H_{2n-16}^O$	Dibenzofurans
		$C_n H_{2n-18}^O$	Hydroxyanthracenes
		$C_n H_{2n-20}^O$	Hydroxynaphthenoanthracenes
		$C_n H_{2n-22}^O$	Hydroxypyrenes

$C_n H_{2n-24} O$	Hydroxychrysenes	$C_n H_{2n-6} O_2$	Dihydroxybenzenes
$C_n H_{2n-26} O$	Hydroxycholanthrenes	$C_n H_{2n-8} O_2$	Dihydroxyindanes
$C_n H_{2n-28} O$	Hydroxybenzopyrenes	$C_n H_{2n-10} O_2$	Hydroxybenzofurans
$C_n H_{2n-30} O$	Hydroxypicenes	$C_n H_{2n-12} O_2$	Dihydroxytetralins
$C_n H_{2n-32} O$	Hydroxyanthanthrenes	$C_n H_{2n-14} O_2$	Hydroxyindenofurans
$C_n H_{2n-38} O$	Hydroxybenzanthanthrenes	$C_n H_{2n-16} O_2$	Hydroxydibenzofurans
$C_n H_{2n-5} N$	Pyridines	$C_n H_{2n-18} O_2$	Dihydroxyanthracenes
$C_n H_{2n-7} N$	Naphthenopyridines	$C_n H_{2n-20} O_2$	Dihydroxynaphthoanthracenes
$C_n H_{2n-9} N$	Indoles	$C_n H_{2n-22} O_2$	Dihydroxypyrenes
$C_n H_{2n-11} N$	Quinolines	$C_n H_{2n-24} O_2$	Dihydroxychrysenes
$C_n H_{2n-13} N$	Naphthoquinolines	$C_n H_{2n-26} O_2$	Dihydroxycholanthrenes
$C_n H_{2n-15} N$	Carbazoles	$C_n H_{2n-8} SO$	Hydroxycyclopentenothiophenes
$C_n H_{2n-17} N$	Acridines	$C_n H_{2n-10} SO$	Hydroxybenzothiophenes
$C_n H_{2n-19} N$	Naphthenobenzoquinolines	$C_n H_{2n-12} SO$	Hydroxynaphthenobenzothiophenes
$C_n H_{2n-21} N$	Benzocarbazoles	$C_n H_{2n-16} SO$	Hydroxydibenzothiophenes
$C_n H_{2n-23} N$	Benzacridines	$C_n H_{2n-18} SO$	Hydroxynaphthenonaphthothiophenes
$C_n H_{2n-25} N$	Naphthenobenzacridines	$C_n H_{2n-20} SO$	Hydroxyfluorenoothiophenes
$C_n H_{2n-27} N$	-	$C_n H_{2n-16} O_3$	Dihydroxydibenzofurans
$C_n H_{2n-29} N$	-	$C_n H_{2n-10} SO_2$	Dihydroxybenzothiophenes
$C_n H_{2n-31} N$	-	$C_n H_{2n-16} SO_2$	Dihydroxydibenzothiophenes
		$C_n H_{2n-18} SO_2$	Dihydroxynaphthenonaphthothiophenes
		$C_n H_{2n-20} SO_2$	Dihydroxyfluorenoothiophenes

The model structures listed above were deduced by observing the molecular weight of the first member for each compound type in a large number of samples. This observed molecular weight was in most cases identical to that of the model structures proposed. As isomeric compound types of the same nuclear molecular weight, such as anthracenes and phenanthrenes, cannot be separated by mass spectrometric means, these structures should be considered only indicative.

Additional compound types have been of course detected in other samples. The most interesting among these were compounds as condensed as  $C_n H_{2n-48}$ ,  $C_n H_{2n-42} O$ ,  $C_n H_{2n-34} O_2$ ,  $C_n H_{2n-32} SO$ , and several compound types containing NO, and S<sub>2</sub> groups.

The presence of O, O<sub>2</sub> groups, most probably in the hydroxyl form, is considered quite revealing, particularly in view of the fact that these hydroxyl groups are located on hydrocarbons containing up to 8 aromatic rings. The detection of these very condensed heterocompounds in coal liquefaction products corroborates the views on coal structure, reported by Hill (8). According to this and other authors, coal is viewed as a polymer composed of polyaromatic nuclei linked by -O- and -S- bridges.

It is reasonable to expect that these linkages break upon hydrogenation, thus giving rise to the polyaromatic phenols detected in our analyses.

Another interesting insight in the structure of coal is provided by the analysis of the heavier fractions (700°F.+) of hydrogenated material. As shown by the example reported below, these materials contain considerable amounts of polynuclear aromatics, associated with as many as a total of fifteen to twenty C atoms in side chains. It is conceivable, of course, that naphthenoaromatic nuclei are also present. It is believed that these side chains are short, with one or two C atoms per side chain, although due to the insolubility of this type of material in any solvent, this assumption could not be confirmed by NMR techniques. These short side chains could be derived from hydrocracking of naphthenoaromatic compounds or from hydrogenation of methylene linkages in the original coal structure.

Analysis of a Heavy Hydrogenated Fraction

<u>Compound Type</u>	<u>Weight Percent</u>	<u>Avg. MW</u>	<u>Compound Type</u>	<u>Weight Percent</u>	<u>Avg. MW</u>
$C_n H_{2n-0}$	0.033	308	$C_n H_{2n-36}$	0.147	379
$C_n H_{2n-2}$	0.077	129	$C_n H_{2n-38}$	0.072	386
$C_n H_{2n-4}$	0.254	185	$C_n H_{2n-40}$	0.013	410
$C_n H_{2n-6}$	0.298	102	$C_n H_{2n-42}$	0.015	415
$C_n H_{2n-8}$	0.792	153	$C_n H_{2n-44}$	0.002	400
$C_n H_{2n-10}$	1.675	195	$C_n H_{2n-4}^S$	0.004	126
$C_n H_{2n-12}$	1.425	228	$C_n H_{2n-16}^S$	0.003	226
$C_n H_{2n-14}$	2.196	236	$C_n H_{2n-18}^S$	0.002	231
$C_n H_{2n-16}$	4.312	248	$C_n H_{2n-20}^S$	0.005	252
$C_n H_{2n-18}$	5.743	270	$C_n H_{2n-10}^O$	0.006	203
$C_n H_{2n-20}$	6.931	286	$C_n H_{2n-12}^O$	0.010	215
$C_n H_{2n-22}$	7.628	282	$C_n H_{2n-14}^O$	0.013	178
$C_n H_{2n-24}$	6.066	302	$C_n H_{2n-16}^O$	0.066	228
$C_n H_{2n-26}$	4.407	322	$C_n H_{2n-18}^O$	0.163	240
$C_n H_{2n-28}$	2.794	327	$C_n H_{2n-20}^O$	0.062	248
$C_n H_{2n-30}$	1.393	340	$C_n H_{2n-22}^O$	0.093	264
$C_n H_{2n-32}$	1.095	341	$C_n H_{2n-24}^O$	0.122	294
$C_n H_{2n-34}$	0.378	365			

$C_n H_{2n-26}^O$	0.125	302	$C_n H_{2n-32}^O$	0.012	356
$C_n H_{2n-28}^O$	0.056	317	$C_n H_{2n-34}^O$	0.004	357
$C_n H_{2n-30}^O$	0.015	328			
Nonvolatile residue 51.50					

Note: This is the routine format, which does not include  $O_2$  or N compounds, and does not separate isomeric hydrocarbons.

Carbon Number Distribution in a Heavy Hydrogenated Fraction

<u>Carbon Number</u>	<u><math>C_n H_{2n-22}</math></u>	<u><math>C_n H_{2n-28}</math></u>	<u><math>C_n H_{2n-32}</math></u>	<u><math>C_n H_{2n-38}</math></u>
16	0.740	-	-	-
17	0.447	-	-	-
18	0.333	-	-	-
19	0.311	-	-	-
20	0.582	0.128	-	-
21	0.760	0.220	-	-
22	0.750	0.218	0.100	-
23	0.685	0.220	0.102	-
24	0.690	0.255	0.074	-
25	0.500	0.295	0.094	-
26	0.475	0.300	0.104	0.007
27	0.370	0.305	0.110	0.005
28	0.330	0.220	0.092	0.006
29	0.243	0.184	0.094	0.012
30	0.165	0.152	0.111	0.006
31	0.135	0.080	0.051	0.006
32	0.040	0.084	0.046	0.007
33	0.044	0.074	0.030	0.008
34	0.028	0.044	0.017	0.012
35	-	0.015	-	0.003
Total	7.628	2.794	1.025	0.072

CONCLUSION

High resolution-low voltage mass spectrometry is thus a very powerful tool for the characterization of coal liquefaction products and for yielding rapid and detailed data useful for process development studies. The method can also be applied to the volatile portions of powdered coal and coal extracts. The data obtained on a great many samples analyzed permitted us to gain some insight into the structure of coal.

ACKNOWLEDGEMENT

The authors wish to thank Mr. G. R. Taylor and Mr. J. L. Taylor who obtained the experimental mass spectral data.

## LITERATURE CITED

1. Lumpkin, H. E., *Anal. Chem.* 36, 2399 (1964).
2. Sharkey, A. G., Jr., Shultz, J. L., Kessler, T., "Procedures of the 15th Annual Conference on Mass Spectrometry and Allied Topics, May 1967, pp. 443-446. ASTM E-14; Denver, Colorado.
3. Kessler, T., Raymond, R. I., Sharkey, A. G., Jr., "Procedures of the 16th Annual Conference on Mass Spectrometry and Allied Topics, May 1968, pp. 356-358. ASTM E-14, Pittsburgh, Pennsylvania.
4. Shultz, J. L., Kessler, T., Friedel, R. A., Sharkey, A. G., Jr., *Ibidem*, pp. 359-361. LJ
5. Johnson, B. H., Aczél, Thomas, *Anal. Chem.* 39, 682, 1967.
6. Aczél, Thomas, Johnson, B. H. Preprints of papers, Division of Petroleum Chemistry, 153rd National Meeting of the American Chemical Society, Miami Beach, Florida, April 1967.
7. Aczél, Thomas, Allan, D. E., Harding, J. H., Knipp, E. A., "Procedures of the 16th Annual conference on Mass Spectrometry and Allied Topics, May 1968, pp. 366, 367. ASTM E-14, Pittsburgh, Pennsylvania.
8. Hill, G. R., Lyon, Lloyd B., *Ind. & Eng. Chem.* 54, 37 (1962).

## CHARACTERIZATION OF IRON MINERALS IN COAL BY LOW-FREQUENCY INFRARED SPECTROSCOPY

Patricia A. Estep, John J. Kovach, Clarence Karr, Jr.,  
Edward E. Childers, and Arthur L. Hiser

Morgantown Coal Research Center, Bureau of Mines,  
U. S. Department of the Interior, Morgantown, West Virginia 26505

The Bureau of Mines, U. S. Department of the Interior, is conducting basic research on minerals occurring in coal to assist in solving problems created by their presence. Of particular interest in these studies are the abundant iron-bearing minerals which are directly linked with air and water pollution, are important in coal combustion, carbonization and hydrogenation, and offer potential for profitable utilization. Iron is second only to aluminum as the most abundant metallic constituent of coal, reflecting its natural abundance in the crust of the earth. Iron is a major element of high-temperature coal ash and ranges from 5 to 35 weight-percent (reported as  $\text{Fe}_2\text{O}_3$ ) for United States bituminous coals (1). Although some of the iron may be organically bound in the coal (2), a large portion is known to occur in a variety of mineral forms.

Previous studies have shown that one of the most effective methods for determining the structure and concentration of coal minerals is low-frequency infrared spectroscopy (3). The application of infrared analysis to a study of iron minerals in coal required a unique compilation of spectral data. Much of the required data was not available from the literature or was of such a poor quality as to be unreliable. In addition, most earlier work did not include the new and useful low-frequency data made available for most minerals by extension of high-resolution commercial infrared instrumentation to  $200\text{ cm}^{-1}$ .

The purpose of this paper is to present the infrared data that we have collected for some iron-bearing minerals in bituminous coal, in both their original and altered forms, and to demonstrate the usefulness of this data for analysis of a variety of typical bituminous coal mineral samples. While iron minerals not included here may occur in coal, the iron minerals for this study were selected on the basis of their frequency of occurrence in samples examined at the Morgantown Coal Research Center and in coals described in the literature.

### EXPERIMENTAL

To prepare the standard spectra required for this work, several specimens of each of the iron minerals were obtained from different localities. Milligram amounts of each of these samples were selected with a stereomicroscope under 10-60X magnification. As an aid in isolation of pure specimens, we made extensive use of microchemical and determinative mineralogy tests. The purities of specimens were verified from x-ray powder diffraction data and from infrared literature data, when available. These checks showed that many of the mineral samples had been incorrectly identified by the supplier. Several minerals were obtained as pure synthetic polycrystalline phases from Tem-Pres Research, Inc., State College, Pa., and infrared spectra of these synthetic minerals were used as further purity checks on natural mineral specimens.

Pellets for infrared analysis were prepared by hand blending one milligram of the preground mineral with 500 milligrams of powdered cesium iodide (Harshaw) for five minutes in a mullite mortar. This mixture was triple pressed in a die at 23,000 pounds total load, with a 15 minute total press time. Pellets were scanned immediately on a Perkin-Elmer 621 infrared grating spectrophotometer purged with dry air. Further considerations in solid state sampling of minerals for infrared analysis have been treated in an earlier publication (3). Coal minerals to be analyzed by infrared were enriched by a variety of techniques. Low-temperature ashing, under 150° C, in an oxygen plasma produced by an r. f. field of 13.56 MHz, for example, gave essentially unaltered mineral residues from coal. In addition, conventional gravity and magnetic separation methods and hand selection with a microscope were used.

## RESULTS AND DISCUSSION

Sulfides. Iron disulfides, pyrite and marcasite ( $\text{FeS}_2$ ), the most abundant iron-bearing minerals in coal, contain much reactive sulfur and thus are major contributors to air and water pollution. These dimorphs (cubic and orthorhombic, respectively) can be identified and differentiated by their infrared spectra in the low-frequency region only (3). Spectral differences, shown in Figure 1 and Table 1, were used to demonstrate that pyrite predominates in the bituminous coals investigated in this work. The detection and determination of pyrite by infrared spectroscopy has been helpful in research on methods for its removal from coal. Gravity separation methods are frequently employed and Figure 2 demonstrates the enrichment of pyrite in the 2.9 specific gravity sink fraction of a mine refuse sample from a West Virginia bituminous coal. The 1.7 specific gravity fraction, curve (a), is shown here to point out that absorption bands from other commonly occurring coal minerals, e. g., kaolinite, may overlap those of pyrite and thus decrease its detectability in mixtures not subjected to separation methods.

Pyrrhotite ( $\text{Fe}_{1-x}\text{S}$ ) is an iron sulfide found in coal (4) and in coal ash slag, where it had been produced from the breakdown of pyrite (5). We did not detect infrared absorption bands out to  $17\text{ cm}^{-1}$  for either the monoclinic or hexagonal crystalline forms of pyrrhotite, hence it is possible that this mineral cannot be determined in natural mixtures by infrared spectroscopy. We have not identified it in any of our bituminous coal samples examined to date by x-ray diffraction analysis.

The iron-bearing sulfide mineral, chalcopyrite (tetragonal,  $\text{CuFeS}_2$ ), has been identified in coal (6, 7). It is known to be the most widely occurring copper mineral and is commonly associated with pyrite ores. Figure 3 and Table 1 show that its absorption bands are shifted to lower frequencies from the corresponding bands for pyrite. These data are in good agreement with those of Gillieson (8).

Carbonates. The carbonate mineral, siderite ( $\text{FeCO}_3$ ), has been identified in coal and is believed to have been formed at the time of burial of plant remains (9). Weathering can convert it to limonite which can then lose water to produce hematite. Siderite has been identified in coals from wide geographic localities and varying ranks. Figure 4 demonstrates its detection in a Virginia bituminous coal. Here, siderite is seen to be the major constituent of a heavy sink fraction from fine coal washing. Adler (10) and Hunt (11) have presented the infrared

spectrum for siderite to  $625\text{ cm}^{-1}$  and Angino (12) has published its infrared data only in the low-frequency region below  $500\text{ cm}^{-1}$ . The distinction of siderite from other possible coal mineral carbonates was facilitated through use of the complete infrared spectrum, as shown in Figure 4, containing all relative intensity information.

Another common iron carbonate often found in coal is ankerite (6, 13, 14). Infrared data has been presented for ankerite by Huang (15) to  $667\text{ cm}^{-1}$  and by Moenke (16) to  $500\text{ cm}^{-1}$ . Both workers utilized very minor band shifts (3 to  $5\text{ cm}^{-1}$ ) for distinguishing ankerite from the isostructural members of its group, and attributed these shifts to cation substitution effects. In a recent study of the carbonate minerals in coal (17) we examined seven ankerite samples from different localities. We observed no detectable frequency shifts in the carbonate fundamentals from those of dolomite. In the low-frequency lattice vibration region, however, there was a general broadening of bands and other detectable changes. In going from dolomite to ankerite, the  $252\text{ cm}^{-1}$  dolomite band was reduced in intensity, the  $312\text{ cm}^{-1}$  band was reduced in intensity and shifted to higher frequency, and the  $391\text{ cm}^{-1}$  shoulder was less resolved. This mineral was frequently misidentified by the supplier because five additional samples of ankerite that we examined were shown by infrared and x-ray analysis to be siderite.

Oxides and Hydrus Oxides. The iron oxides, hematite and magnetite, and the hydrous iron oxides goethite and lepidocrocite have all been identified in coal by petrographic or x-ray methods (18). These may occur in coal as original minerals or as products of weathering of iron-bearing minerals. Very little reliable infrared data is available in the literature for these oxides. Absorption bands for hematite, reported in the  $1000\text{-}1110\text{ cm}^{-1}$  region by Hunt (11) and Omori (19), are in error, as none of the anhydrous oxides absorb above  $600\text{ cm}^{-1}$ . The infrared spectrum of hematite presented by Liese (20) contains absorption bands due to an impurity, and our data indicate that his sample contained maghemite. Recently, infrared spectra for iron oxides, available as commercial chemicals, have been presented to  $200\text{ cm}^{-1}$  by Afremow (21) and McDevitt (22). The spectra we obtained for naturally occurring mineral samples are only in partial agreement with the data in these two references. For example, the distinction between  $\alpha\text{Fe}_2\text{O}_3$  (hematite, trigonal) and  $\gamma\text{Fe}_2\text{O}_3$  (maghemite, cubic) is not readily apparent from the spectra presented in either paper. Our spectra for these dimorphs, Figure 5, show frequency differences for all three major absorption bands. These shifts were found to be consistent for several samples from different localities and are believed to be reliable. For magnetite ( $\text{Fe}_3\text{O}_4$ ), Liese (20) reports (to  $300\text{ cm}^{-1}$ ) only one absorption band at  $570\text{ cm}^{-1}$  for a number of naturally occurring magnetite specimens. Our magnetite spectrum, Figure 5, with two absorption bands, is in better agreement with that presented by Afremow (21) for the black iron oxide ( $\text{Fe}_3\text{O}_4$ ). The conversion of magnetite through maghemite to hematite can be readily followed by use of their spectral differences, shown in Figure 5.

The iron oxide, wüstite (essentially  $\text{FeO}$ ), is an alteration product of the iron minerals in coal, and has been found in coal ash slags and fly ash. The spectrum of a nonstoichiometric, single phase sample of synthetic wüstite exhibits only one broad absorption band at  $375\text{ cm}^{-1}$ .

The titanium containing iron oxide, ilmenite (trigonal,  $\text{FeTiO}_3$ ), which is frequently associated with hematite and magnetite, has been identified in coal (23). Titanium commonly occurs in United States bituminous coals (1), and shows a close correspondence to its natural abundance in the earth's crust. Hunt (11) and Omori (19) report infrared absorption bands for ilmenite in the region above  $625 \text{ cm}^{-1}$  which are undoubtedly in error. Liese (20) found three strong absorption bands, all in the low-frequency region, that differ as the Ti/Fe ratio varies. He shows these bands to shift systematically from 540, 461, and  $325 \text{ cm}^{-1}$  to 532, 440, and  $295 \text{ cm}^{-1}$  as Ti increases and Fe decreases. He points out that this frequency shift is not in the expected direction and suggests that the presence of intergrown hematite may be causing this effect. Data from our laboratory support his intergrowth interpretation. Our spectra for ten samples of ilmenite from various localities show consistent band positions at 525 (s), 438 (m), and  $300 \text{ (s) cm}^{-1}$ . Figure 6 shows the spectrum of a sample from Norway. This spectrum agrees better with Liese's set of lower frequency bands, while his set of higher frequency bands agrees better in frequency and shape with our hematite data.

Adler (24) and White (25) have shown that the hydrous oxide dimorphs goethite,  $\alpha\text{FeO}(\text{OH})$ , and lepidocrocite,  $\gamma\text{FeO}(\text{OH})$ , both orthorhombic, can be readily distinguished by differences in the  $4000\text{-}600 \text{ cm}^{-1}$  region. Figure 7 shows their marked spectral differences and presents additional data for the low-frequency region to  $200 \text{ cm}^{-1}$ . A further useful distinction between these dimorphs is their behavior on heating. Goethite dehydrates to form paramagnetic hematite while lepidocrocite dehydrates on heating to form ferromagnetic maghemite. We used these conversions for further verification of the spectra for all four forms. The absence of vibrations due to OH groups considerably simplifies the infrared spectrum, as shown by a comparison of Figures 5 and 7.

We have frequently identified the oxides of iron and their hydrous forms in samples obtained by magnetic separations from coal. For example, Figure 8 demonstrates the detection of substantial amounts of goethite in the magnetic fraction from a mine refuse sample from a West Virginia bituminous coal. The highly characteristic goethite bands at  $800$  and  $900 \text{ cm}^{-1}$ , assigned by White (25) to an OH bending vibration and an Fe-O stretching mode, respectively, are particularly useful because this doublet occurs in a range not extensively overlapped by bands of other common mineral components. Similarly, the weaker bands at 215, 358, and  $1018 \text{ cm}^{-1}$ , seen in the spectrum of the magnetic fraction in Figure 8, can be assigned to minor amounts of lepidocrocite. The capability of infrared spectroscopy for distinguishing between goethite and lepidocrocite can be applied to the determination of the mineralogical composition of limonite,  $\text{FeO}(\text{OH}) \cdot x\text{H}_2\text{O}$ , an amorphous mixture of hydrous iron oxides with variable water content that is difficult to characterize by x-ray diffraction. We have observed goethite to be the predominant species in several limonite specimens from a variety of world localities. Limonite has frequently been reported to be present in coal as a product of weathering.

Other types of coal product samples typically containing iron oxides as alteration products of original iron minerals are combustion products such as fly ash, boiler deposits, conventional high-temperature ash residues from coal, and burned mine refuse. Figure 9, curve (c), for example, demonstrates the extensive oxidation of pyrite to hematite in a sample of burned mine refuse from a West Virginia bituminous coal. The sample, obtained from a burning coal refuse bank, was

pulverized and subjected to float sink separations. The infrared spectrum of the 2.9 specific gravity sink fraction shows hematite to be predominant, with only minor amounts of pyrite remaining. This particular analysis demonstrates the necessity for using the low-frequency region, 600-200  $\text{cm}^{-1}$ , because there were no major absorptions above 600  $\text{cm}^{-1}$  in the refuse sample. Comparison of curves (a) and (b) for pyrite and hematite shows that the specificity of their absorption bands affords an excellent opportunity for quantitative analysis and thus determination of degree of oxidation by burning or weathering.

$\text{Fe}(\text{OH})_3$ , a hydrolysis product of ferric sulfates, known as "yellow boy," is frequently precipitated from alkaline streams containing drainage from coal mines. Although this compound exhibits a rather diffuse infrared spectrum, we have used its broad absorption bands centered at 450, 575, 675, and 3450  $\text{cm}^{-1}$  for identification. We have been unable to find any infrared data to 200  $\text{cm}^{-1}$  for this compound in the literature.

Sulfates. Iron sulfates occur in coals primarily as oxidation products of the iron sulfides, and various forms can be produced, depending on weathering conditions. Anhydrous  $\text{FeSO}_4$ , or its various hydrates, can easily form and be converted by further oxidation into  $\text{Fe}_2(\text{SO}_4)_3$  or any of its possible hydrates. Nufer (26), by x-ray diffraction, has determined that the species typically found in West Virginia bituminous coal are principally szomolnokite,  $\text{FeSO}_4 \cdot \text{H}_2\text{O}$ , and melanterite,  $\text{FeSO}_4 \cdot 7\text{H}_2\text{O}$ . Iron sulfates are associated with water pollution problems resulting from mine drainage, coal processing plants, and weathered refuse banks (27). The infrared spectra that we obtained for a number of samples from these sources showed different hydration states for the iron sulfates. For example, the surface film from a sample of coal mine refuse is seen from its infrared spectrum in Figure 10, curve (c), to be predominantly anhydrous iron sulfate, indicating oxidation in a very dry atmosphere. Minor amounts of the hydrated forms of ferrous sulfates and pyrite were also present in this sample. When considerable atmospheric moisture is present, the surface film on pyrite-rich mine refuse was usually identified as melanterite, as seen in Figure 11.

Hydrous iron sulfates are another class of minerals for which very little reliable infrared data is available in the literature. Adler (28) has presented the infrared spectrum of szomolnokite only to 800  $\text{cm}^{-1}$ . Omori (29) has published poorly resolved infrared spectra for siderotil,  $\text{FeSO}_4 \cdot 5\text{H}_2\text{O}$ , melanterite, and coquimbite,  $\text{Fe}_2(\text{SO}_4)_3 \cdot 9\text{H}_2\text{O}$ , only to 600  $\text{cm}^{-1}$ . Infrared data for the synthetically prepared forms of  $\text{FeSO}_4 \cdot 7\text{H}_2\text{O}$  and  $\text{Fe}_2(\text{SO}_4)_3 \cdot x\text{H}_2\text{O}$  have been presented by Miller (30, 31) to 300  $\text{cm}^{-1}$  and Sadtler (32) to 400  $\text{cm}^{-1}$ . However, no systematic study has been made of the various hydrated sulfates of  $\text{Fe}^{2+}$  or  $\text{Fe}^{3+}$  showing the dependency of the infrared spectrum on additions of water to the crystal lattice. In the present work, infrared spectra were obtained for samples of naturally occurring and microscopically identified iron sulfate minerals. These included iron in both ferrous and ferric states and in the commonly found hydrated forms. The hydration states of some of these iron sulfate minerals are known to be easily altered (33). However, variations of temperature and relative humidity in our pellet preparation produced no detectable spectral changes. The spectral data for these minerals are shown in Tables 2 and 3, with their tentative vibrational assignments. In the absence of data for several intermediate hydrates, and the possibility of mixed crystalline phases for some samples, it was not possible to make any rigorous spectral-structural correlations. However, several spectral

differences among these minerals were observed and used in identifications. For example, the marked spectral differences allowing a distinction between anhydrous ferrous sulfate and one of its hydrated forms, melanterite, are shown in Figure 10, curve (b), and in Figure 11, curve (a). The weak OH absorptions appearing in the spectrum of the anhydrous form agree with those in the monohydrate and may be due to small amounts of this form.

Some systematic spectral variations were noted for lattice water vibrations. For example, the ferrous sulfate hydrate system (Table 2) showed the expected systematic increase in intensity of the OH stretching and HOH deformation modes with an increasing number of lattice water molecules. Absorption for ferrous sulfate hydrates in the OH stretching region showed two to four components, while absorption for ferric sulfate hydrates in this region was asymmetrically broadened to one band and generally shifted to lower frequencies. The frequency for the HOH deformation mode remained essentially independent of the amount of water present. It appeared near  $1620\text{ cm}^{-1}$  (usually split) for the ferrous sulfate hydrates, but shifted to a higher frequency position near  $1640\text{ cm}^{-1}$  for the ferric sulfate hydrates.

The fundamental vibrations of the sulfate ion,  $\nu_1$ ,  $\nu_3$ , and  $\nu_4$ , as tentatively assigned in Tables 2 and 3 for iron sulfates, all indicate lower symmetry than that of the free tetrahedral ion. Ross (34) has discussed the reasons for lower symmetry of the sulfate ion in the solid state. When this occurs, degeneracies are removed and new selection rules allow forbidden vibrations to appear. For example, the degenerate  $\nu_3$  sulfate group vibration appears as a triplet in all samples examined. The  $\nu_1$  appears in all spectra, although it shows a substantially reduced intensity when just one water molecule is added. The frequency variations for the sulfate fundamentals are not systematic with additions of lattice water and changes in the oxidation state of the iron. However, the observed spectral variations for these iron sulfates, in spite of their irregularities, can be of diagnostic value and can provide a basis for identification of an individual compound.

#### ACKNOWLEDGMENT

The authors are grateful to John S. White, Division of Mineralogy, Smithsonian Institution, Washington, D. C., and R. I. Gait, Royal Ontario Museum, Toronto, Canada, who supplied several samples of hydrated iron sulfates, and to John J. Renton, Geology Department, West Virginia University, Morgantown, who provided x-ray data on mineral samples.

#### LITERATURE CITED

1. Selvig, W. A., and F. H. Gibson, BuMiner Bull. 567 (1956), 33 pp.
2. Lefelhocz, J. F., R. A. Friedel, and T. P. Kohman, Geochim. Cosmochim. Acta 31, 2261 (1967).
3. Estep, P. A., J. J. Kovach, and C. Karr, Jr., Anal. Chem. 40, 358 (1968).

4. Sen, P., and A. N. Roy, *J. Mines, Metals, Fuels* 10, 7 (1962).
5. Watt, J. D., *Brit. Coal Util. Res. Assoc., Monthly Bull.* 26, No. 2, 49 (1959).
6. Kemezys, M., and G. H. Taylor, *J. Inst. Fuel* 37, 389 (1964).
7. Bethell, F. V., *Brit. Coal Util. Res. Assoc., Monthly Bull.* 26, No. 12, 401 (1962).
8. Gillieson, A. H., Dept. of Energy, Mines, and Resources, Ottawa, Ontario, Canada, private communication (1968).
9. Smyth, M., *Fuel* 45, 221 (1966).
10. Adler, H. H., and P. F. Kerr, *Am. Mineralogist* 48, 124 (1963).
11. Hunt, J. M., M. P. Wisherd, and L. C. Bonham, *Anal. Chem.* 22, 1478 (1950).
12. Angino, E. E., *Am. Mineralogist* 52, 137 (1967).
13. Dixon, K., E. Skipsey, and J. T. Watts, *J. Inst. Fuel* 37, 485 (1964).
14. Brown, H. R., R. A. Durie, and H. N. S. Schafer, *Fuel* 34, 59 (1960).
15. Huang, C. K., and P. F. Kerr, *Am. Mineralogist* 45, 311 (1960).
16. Moenke, H., *Infrared Phys.* 2, 111 (1962).
17. Estep, P. A., J. J. Kovach, A. L. Hiser, and C. Karr, Jr., Ch. in "Spectrometry of Fuels and Related Materials," ed. by R. A. Friedel, Plenum Press, New York, N. Y., 1969 (in press).
18. Rekus, A. F., and A. R. Haberkorn, III, *J. Inst. Fuel* 39, 474 (1966).
19. Omori, K., *Sci. Rept. Tohoku Univ., Third Ser.* 9, 65 (1964).
20. Liese, H. C., *Am. Mineralogist* 52, 1198 (1967).
21. Afremow, L. C., and J. T. Vandenberg, *J. Paint Tech.* 38, 169 (1966).
22. McDevitt, N. T., and W. L. Baun, *Spectrochim. Acta* 20, 799 (1964).
23. Alekseev, L. S., *Geomorjol, Paleogeogr., Geol., Polezn. Iskop. Priamur'ya, Dal'nevost. Filial Sibirsk. Otd. Akad. Nauk SSSR* 21, (1964).
24. Adler, H. H., *Econ. Geol.* 58, 558 (1963).
25. White, W. B., and R. Roy, *Am. Mineralogist* 49, 1670 (1964).
26. Nufer, E. B., Master's Thesis, West Virginia University (1967), 73 pp.

27. Lorenz, W. C., BuMiner. Inf. Circ. 8080 (1962), 40 pp.
28. Adler, H. H., and P. F. Kerr, *Am. Mineralogist* 50, 132 (1965).
29. Omori, K., and P. F. Kerr, *Geol. Soc. Am. Bull.* 74, 709 (1963).
30. Miller, F. A., and C. H. Wilkins, *Anal. Chem.* 24, 1253 (1952).
31. Miller, F. A., G. L. Carlson, F. F. Bentley, and W. H. Jones, *Spectrochim. Acta* 16, 135 (1960).
32. Sadtler Research Laboratories, Philadelphia, Pa. *High Resolution Spectra of Inorganics and Related Compounds* 1 (1965), Supplement, (1967).
33. Ehlers, Ernest G., and D. V. Stiles, *Am. Mineralogist* 50, 1457 (1965).
34. Ross, S. D., *Spectrochim. Acta* 18, 1575 (1962).

Table 1. - Infrared Absorption Bands for Common Iron Minerals

Mineral	Frequency, $\text{cm}^{-1}$ <sup>a</sup>
Pyrite (Gilman, Eagle County, Colorado)	284 (w), 340 (m), 391 (vw), 411 (s)
Marcasite (Ottawa County, Oklahoma)	285 (w), 321 (m), 350 (m), 396 (s), 412 (s), 422 (vw)
Chalcopyrite (Messina, Transvaal, South Africa)	268 (w), 315 (m), 351 (s), 365 (sh)
Siderite (Washington, Connecticut)	~200 (w), 316 (s), 728 (m), 858 (m), 1410 (s)
Hematite (Ironton, Minnesota)	330 (s), 370 (sh), 470 (m), 550 (s)
Maghemite (LaCodocera, Badajoz, Spain)	320 (s), 451 (m), 530 (s)
Magnetite (Iron Mountain, Utah)	385 (s), 575 (s)
Wüstite (Synthetic, Tem-Pres Research, Inc.)	375 (s)
Ilmenite (Kragersö, Norway)	300 (s), 325 (sh), 438 (m), 525 (s), 675 (sh)
Goethite (Cary Mine, Ironwood, Gogebic County, Michigan)	248 (w), 280 (s), 385 (w), 402 (s), 450 (sh), 568 (m), 662 (w), 800 (m), 900 (m), 3095 (m), 3430 (b)
Lepidocrocite (Fellinghausen, Hessen, Germany)	215 (w), 275 (m), 358 (s), 480 (s), 740 (m), 1018 (m), ~3000 (b), ~3350 (b)

<sup>a</sup> s = strong; m = medium; w = weak; sh = shoulder; b = broad.

Table 2. - Infrared Absorption Bands for Ferrous Sulfate Minerals,  $\text{cm}^{-1}$ 

Tentative assignments	Anhydrous ferrous sulfate $\text{FeSO}_4$ Orthorhombic Fisher Chem. Co.	Szomolnokite $\text{FeSO}_4 \cdot \text{H}_2\text{O}$ Monoclinic Dividend, Utah	Rozenite $\text{FeSO}_4 \cdot 4\text{H}_2\text{O}$ Monoclinic Ontario, Can.	Siderotil <sup>b</sup> $\text{FeSO}_4 \cdot \text{SH}_2\text{O}$ Crystal system undetermined	Melanterite $\text{FeSO}_4 \cdot 7\text{H}_2\text{O}$ Monoclinic Honshu, Japan
OH stretch, lattice water	3410 (w) 3250 (w)	3420 (m) 3240 (sh)	3430 (ms) 3250 (sh)	3448 (ms)	3530 (sh) 3455 (s) 3390 (sh) 3260 (sh)
HOH bend, lattice water	1490 (w)	1650 (w) 1620 (w) 1490 (w)	1620 (w) 1505 (w)	1622 (mw)	1650 (sh) 1618 (m)
$\gamma_3$ , sulfate	1150 (s) 1135 (s) 1076 (m)	1165 (m) 1125 (s) 1095 (m)	1175 (sh) 1140 (s) 1100 (m)	1143 (sh) 1099 (s)	1140 (m) 1105 (s) 1085 (sh)
$\gamma_1$ , sulfate	1010 (m)	1015 (m)	1020 (m)		988 (w)
$\gamma_4$ , sulfate	815 (m) 660 (m) 618 (m) 595 (m)	830 (mw) 660 (m) 620 (m) 599 (m)	860 (mw) 670 (m) 627 (m) 607 (m)	862 (w)	605 (m)
	525 (m) 290 (m) 270 (m) 210 (m)	522 (m) 290 (m) 270 (m) ~ 200 (m)	560 (m) 470 (w) 340 (w) 275 (m)		510 (w) 425 (w) 330 (w)

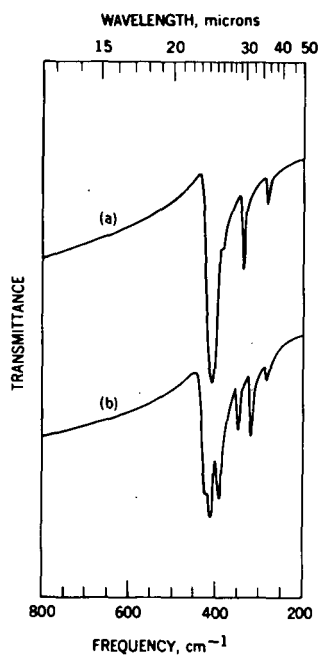
<sup>a</sup> s = strong, m = medium, w = weak, sh = shoulder, b = broad.

<sup>b</sup> Approximate values read from Omori and Kerr (see Ref. 29).

Table 3. - Infrared Absorption Bands for Ferric Sulfate Minerals,  $\text{cm}^{-1}$ <sup>a</sup>

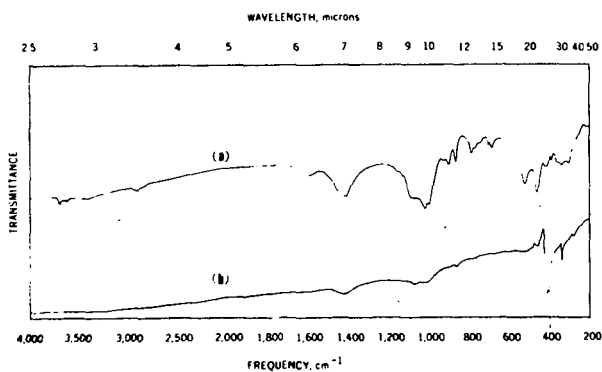
Tentative assignments	Kornelite $\text{Fe}_2(\text{SO}_4)_3 \cdot 7\text{H}_2\text{O}$ Monoclinic Inyo County, Cal.	Coquimbite $\text{Fe}_2(\text{SO}_4)_3 \cdot 9\text{H}_2\text{O}$ Hexagonal San Rafael Swell, Utah	Romerite $\text{Fe}_3(\text{SO}_4)_4 \cdot 14\text{H}_2\text{O}$ Triclinic Trinity County, Cal.	Ferric sulfate $\text{Fe}_2(\text{SO}_4)_3 \cdot x\text{H}_2\text{O}$ J. T. Baker Chemical Co.
OH stretch, lattice water	3410 (s, b)	3300 (s, b)	3300 (s, b)	3360 (s, b), 3200 (sh)
HOH bend, lattice water	1640 (w)	1640 (w)	1640 (w)	1645 (m) 1610 (sh)
$\gamma_3$ , sulfate	1185 (sh) 1115 (s) 1050 (sh)	1165 (s) 1105 (s) 1065 (sh)	1129 (s) 1105 (s) 1085 (sh)	1150 (m) 1105 (s) 1052 (m)
		1023 (w)		
$\gamma_1$ , sulfate	990 (w)	1010 (w)	982 (w)	
	810 (w) 685 (w) 650 (w)	940 (w) 820 (w) 685 (w)	750 (w, b)	800 (w)
$\gamma_4$ , sulfate	595 (m)	608 (sh) 590 (m) 575 (sh)	626 (m) 605 (sh)	630 (sh) 595 (m)
	270 (w)	480 (w) 440 (w) 330 (w) 270 (w)	480 (w) 450 (w) 335 (w) 270 (w) 225 (w)	550 (m) 335 (w) 300 (w) 272 (w)

a s = strong; m = medium; w = weak; sh = shoulder; b = broad.



(a) Pyrite (Colorado)  
 (b) Marcasite (Oklahoma)

FIGURE 1. - Infrared Spectra for Iron Disulfide Dimorphs.



a. "Clay Fraction", 1.7 s.g. slm / kaolinite, quartz, calcite)  
 b. "Iron Fraction", 2.8 s.g. slm / pyrite

FIGURE 2. - Gravity Separation of Slurry Pond Refuse from a W. Va. Bituminous Coal.

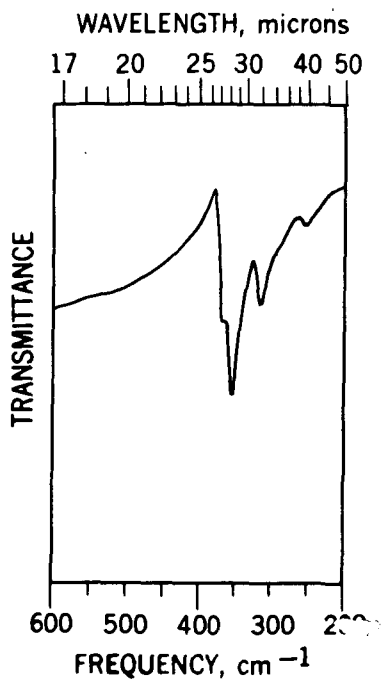
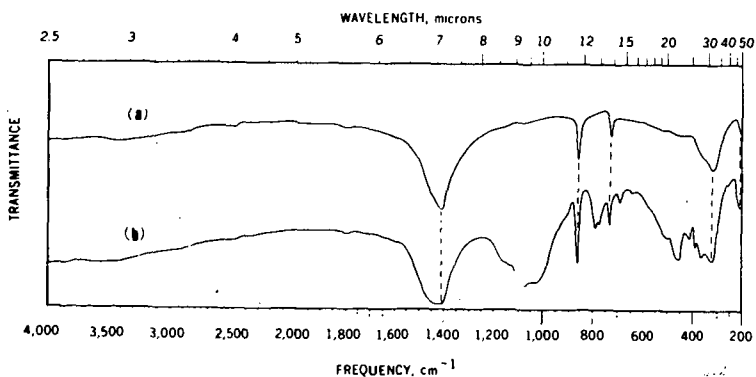


FIGURE 3. - Infrared Spectrum of Chalcopyrite from Messina, Transvaal, South Africa



- (a) Siderite (Connecticut)
- (b) Heavy sink fraction from the fine coal washing, 2.9 s.g. sink

FIGURE 4. - Identification of Siderite from a Virginia Bituminous Coal

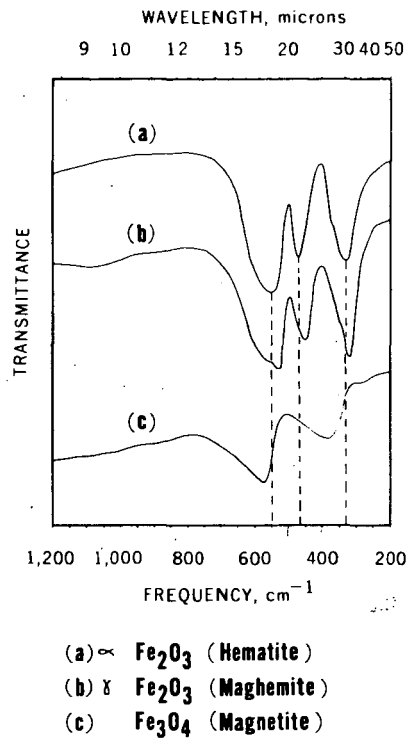


FIGURE 5. - Infrared Spectra of Iron Oxides

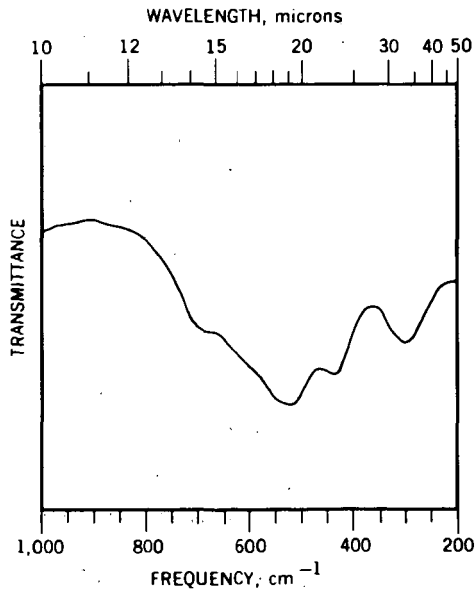


FIGURE 6. - Infrared Spectrum of Ilmenite (Norway)

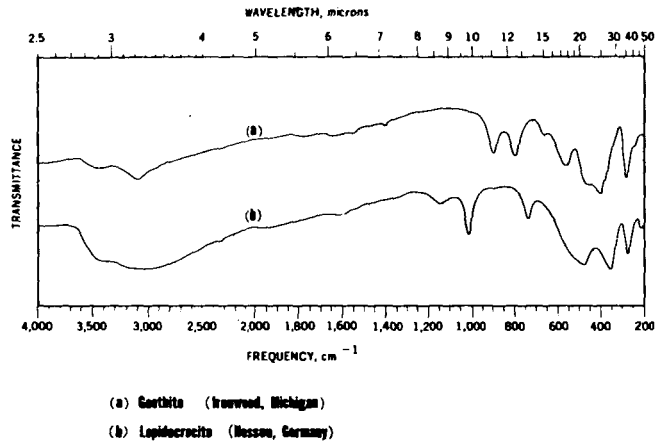


FIGURE 7. - Infrared Spectra of Hydrrous Iron Oxide Polymorphs

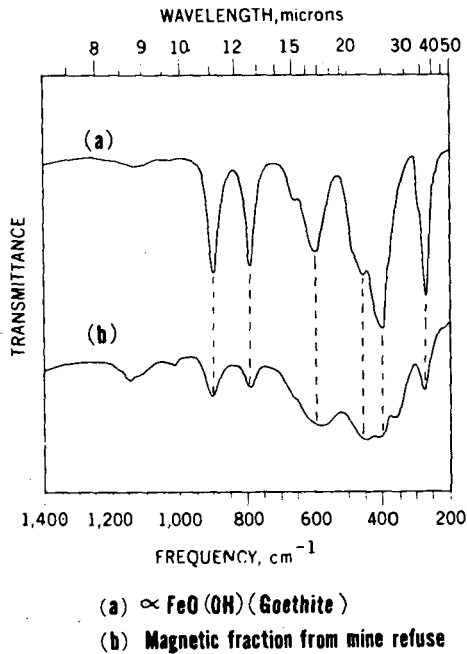
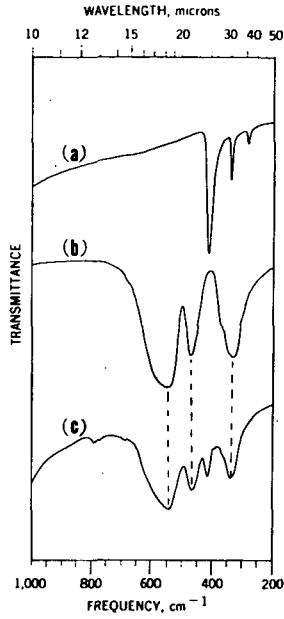


FIGURE 8. - Identification of Goethite in Mine Refuse from a W. Va. Bituminous Coal



- (a) Pyrite (Gilman, Colorado)  
 (b) Hematite (Ironton, Minnesota)  
 (c) Burned mine refuse

FIGURE 9. - Conversion of Pyrite to Hematite in Mine Refuse by Burning

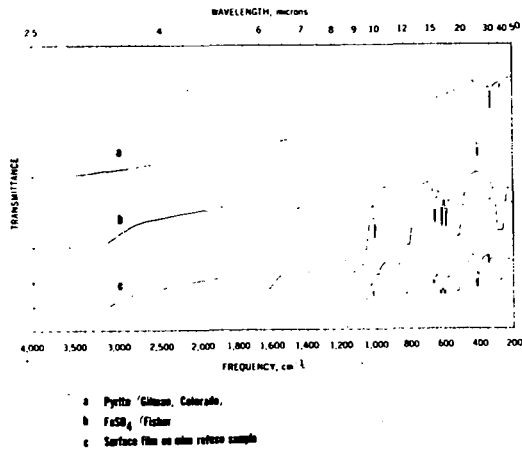


FIGURE 10. - Surface Oxidation of Pyrite from Coal Refuse in a Dry Atmosphere

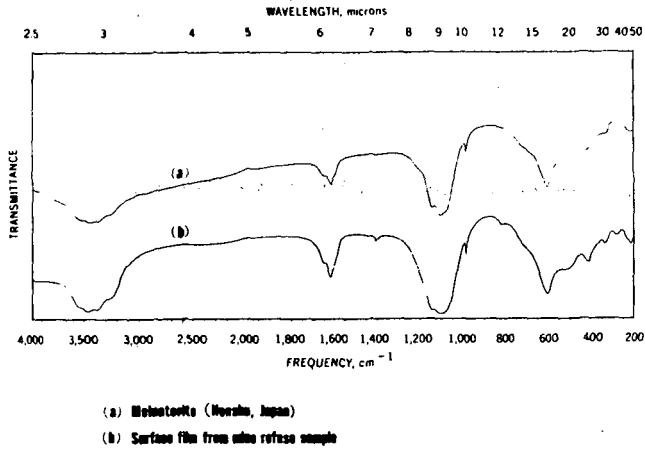


FIGURE 11. - Surface Oxidation of Mine Refuse in a Moist Atmosphere

## DIRECT DETERMINATION OF OXYGEN IN COAL

B.S. Ignasiak\*, B.N. Nandi\*\*, D.S. Montgomery\*\*\*

Fuels Research Centre, Mines Branch, Department of Energy, Mines and Resources,  
Ottawa, Ontario, Canada

## INTRODUCTION

There are two known methods for the direct determination of oxygen in organic matter:

- 1) Schütze method (1) and modifications (2,3,4,5,6,7,8)
- 2) Neutron activation method (9,10)

The principle of the Schütze method depends on thermal decomposition of the sample in a temperature range of 1000° - 1150°C, in an oxygen free atmosphere of inert gas. The gaseous products of pyrolysis are carried over a layer of carbon black or lampblack at a temperature 1120°C. At this temperature all oxygen containing products are transformed into CO which is quantitatively oxidized using I<sub>2</sub>O<sub>5</sub> to CO<sub>2</sub>. The oxygen content of the sample for analysis can be calculated from the gain in CO<sub>2</sub> measured gravimetrically or from the gain in I<sub>2</sub> measured volumetrically. Instead of oxidizing CO to CO<sub>2</sub> some authors suggest the determination of CO directly using chromatographic analysis. (5)

Using platinum on lampblack (7) or nickel on lampblack (5) as a catalyst, it is possible to decrease the temperature for the quantitative conversion to carbon monoxide of the products of pyrolysis of the sample.

All modifications of the Schütze method for the direct determination of oxygen are based on the thermal decomposition of the sample in an inert gas. This requires a very pure sweeping gas and therefore rather complicated methods for the purification of this gas. In effect this means that the analysis is much more prolonged.

The determination of oxygen using the neutron activation method has been described many times in detail. (10) This method allows the total concentration of oxygen to be determined in both the organic and inorganic constituents of the sample. The advantages of this method are: the short time of duration of the analysis and the fact that this is a non-destructive type of test. On the other hand the equipment for the determination of oxygen using neutron activation analysis is very expensive and the sample must be relatively large.

---

\* Permanent address: Department of Coal Chemistry, Adam Mickiewicz University, Poznan, Poland.

\*\* Research Scientist, Fuels Research Centre

\*\*\* Head, Fuels Research Centre

Also, if the principal quantity of interest is the oxygen content of the organic matter in the coal, the mineral matter must be removed. This is a rather laborious process.

The recognized methods of determining the oxygen content of coal, based on Schütze (1) Unterzaucher (2) and Burns (8) are slow and require considerable skill to achieve satisfactory levels of accuracy. The method described here is much more rapid and requires considerably less technique.

## EXPERIMENTAL

### Principle of the Method.

A fast and simple method is described for the determination of oxygen in coals. The principle of the method depends on the pyrolysis of a sample at 1050°C in a vacuum, conversion of all oxygen in the pyrolysis products into CO, the determination of the volume of evolved gas and the measurement of the concentration of carbon monoxide in this gas using gas chromatography.

### Apparatus.

The basic part of the determination, which is the pyrolysis and the measurement of the volume of evolved gas is conducted in the apparatus indicated in Figure 1. The part of this apparatus indicated by 1 referred to as the pyrolyser and is used for the pyrolysis of the sample located at a and the evacuation of the catalyst situated at b. As it must withstand relatively high temperature it is made from Vycor glass. The pyrolyser is connected through the unit 2 to a gas burette, capacity 100 ml, by means of heavy rubber tubing. After completion of the pyrolysis, the mercury from the reservoir is introduced into the apparatus through the one-way stopcock c. The pyrolysis is conducted in a hinged tubular electric furnace into which the pyrolyser unit is placed as shown in Figure 2. The additional equipment required for the determination of oxygen includes a vacuum pump and gas chromatograph suitable for the measurement of carbon monoxide. In this investigation a Fisher Partitioner was used with a double column: - hexamethylphosphoramide on Chromosorb P followed by a Linde molecular sieve 13X. Using such a set of columns it was a simple matter to determine whether the conversion process was quantitative or not as the presence of any CO<sub>2</sub> shows that the conversion is incomplete.

The sample for analysis (60 mg - 100 mg) was weighed in the quartz tube 5 whose shape and dimension are presented in Figure 1. With high oxygen content coals such as lignite the sample weight is kept to 60 mg while for anthracite the sample weight is increased to 100 mg.

### Preparation of the Catalyst.

Two hundred gram of lampblack dried at 105°C for 3 hours was mixed in a beaker with a concentrated solution of nickelous nitrate consisting of 991 g  $\text{Ni NO}_3 \cdot 6 \text{H}_2\text{O}$  dissolved in 200 ml of distilled water. The suspension was mixed mechanically and heated to evaporate the water. The heating was stopped when the residue started to solidify. The contents of the beaker were dried for 24 hours at 105°C in an oven. Then, the catalyst was transferred to a Vycor tube swept with argon. The temperature was increased gradually to 1050°C and maintained under these conditions for 5 hours. The catalyst was then cooled and stored in an air-tight container. The particles of the catalyst, 16-60 mesh Tyler, were used for the oxygen determinations.

### Method of Analysis.

Five g of catalyst was introduced into the tube b of the pyrolyser Figure 1. The part a was cleaned carefully to remove all vestiges of catalyst particles and the sample in the quartz tube 5 was introduced into part pyrolyser. The apparatus was assembled, set up on a stand, and evacuated initially for 5 minutes. Then part b of the pyrolyser was inserted into an oven for 30 minutes at 1050°C. Five minutes before the end of this period in which the catalyst was degassed, the apparatus was re-evacuated. At the conclusion of this 5 minute period the tubing b was withdrawn from the furnace and the tubing a was inserted for 10 minutes into a thermostat at a temperature of 70°C to remove traces of moisture from the coal sample. After the tubing b was cold the catalyst was transferred into a by rotating the pyrolyser and the apparatus was disconnected from the vacuum pump using stopcock c. After the pressure dropped to 0.3 mm of Hg, the hinged furnace was opened for some seconds and the tubing a of the apparatus was placed in the furnace as shown in Figure 2 to avoid heating the coal. After some minutes when the temperature stabilized again at 1050°C the furnace was moved very slowly in the direction of the sample. The rate of evolution of the pyrolysis gases from the sample could be observed by eye, and the rate of advance of the furnace was controlled to avoid sudden bursts of gas. The sample was finally advanced to the mid-point of the furnace and retained there for 10 minutes. After this time the pyrolyser was withdrawn from the furnace and 3 to 4 minutes later the mercury from the reservoir was introduced into the apparatus with vibration from 4. The converted pyrolysis gas was displaced into the gas burette. The volume of the gas was measured and the temperature and atmospheric pressure was noted. The concentration of carbon monoxide was determined by withdrawing a sample for gas chromatography.

The concentration of oxygen in analysed sample was calculated from the equation:

$$\%O = \frac{(0.07143)}{G} \left[ \frac{\%CO \cdot P_1 \cdot V_1 \cdot 0.003592}{T_1} - K \right]$$

where: G - weight of sample g ; V<sub>1</sub> - volume of evolved gas (ml)  
(at temperature T<sub>1</sub> pressure P<sub>1</sub>)

P<sub>1</sub> - atmospheric pressure mm Hg.

T<sub>1</sub> - temperature °K; K - volume of CO ml at temperature 273°K,  
pressure 760 mm of Hg obtained from  
pyrolysis of pure chemical compound not  
containing oxygen.

K is a function of the conditions of analysis such as: temperature,  
time of pyrolysis, method of the preparation  
of catalyst, time and temperature of the  
degasification of catalyst. Consequently,  
to obtain reproducible results it is  
important to adhere strictly to the same  
analytical procedure.

#### Results and Discussion.

The proposed method for the direct determination of oxygen in coal was tested on two standard pure compounds, namely, benzoic acid and acetanilide. Comparative analyses by the neutron activation method were performed on these standards. The results presented in Table 1 show that the proposed method can be considered as a basically suitable analytical procedure for the direct determination of oxygen in many organic compounds. Some caution will have to be used in those cases where the component is known to contain elements that will poison the nickel catalyst.

The establishment of this method for the determination of oxygen in coal required finding the temperature of pyrolysis at which essentially all oxygen from organic matter of coal was evolved from the coke. It was found from the determination of the concentration of oxygen by neutron activation in cokes resulting from the pyrolysis of some coals of different rank demineralized according to Radmacher (11), that the temperature of 1050°C is suitable. This is illustrated in Figure 3. Only in the case of anthracite was the concentration of oxygen in cokes pyrolysed at temperatures of 1050°C and 1100°C relatively high, that is to say approximately 0.9%. At the same time the concentration of ash in this particular anthracite after treatment with hydrochloric acid and hydrofluoric acid was surprisingly high as shown in Table 2, Column 7. So it is assumed that the high concentration of oxygen in cokes from pyrolysis of anthracite at 1050°C and 1100°C is related to the inorganic matter in these cokes. It is worth mentioning that the concentrations of oxygen in both these cokes though heated to different temperatures, i.e., 1050 and 1100°C were the same. Had the oxygen been contained in the organic matter some decrease in concentration should have been observed.

Coals of different rank were analysed before and after removal of the mineral matter using the direct method of determining oxygen. The results are shown in Table 2. Here it is evident that the oxygen content of the demineralized samples are in good agreement with those found by neutron activation analysis.

#### ACKNOWLEDGEMENTS

The authors wish to acknowledge the assistance of the Mineral Science Division and Mr. C. McMahon in particular for determining the oxygen content of the coal and coke samples by neutron activation analysis and Mr. M. Pleet for preparing the drawings.

#### REFERENCES

1. Schütze, M. Zeitschr. Anal. Chem. 1939, 118, 245.
2. Unterzaucher, J. Ber. Dtsch. Chem. Ges. 1940, 73B, 391; Analyst. 1952, 77, 584.
3. Kuck, J.A., Andreatch, A.J., Mohns, J.P. Anal. Chem. 1967, 39, 1249.
4. Korszun, M.D. Zaw. Lab. 1941, 10, 241.
5. Tierientiew, A.P., Turkieltaub, A.M., Bondariewska-ja, E.A., Domoczki, L.A. Dokl. Akad. Nauk SSSR. 1963, 148, 1316.
6. Kuzniecowa, L.W., Stolarowa, E.N., Dobyczin, S.L. Ž. Anal. Chim. Russian, 1965, 20, 836.
7. Oita, I.J., Conway, H.S. Analyt. Chem. 1954, 26, 600.
8. Burns, M.S., Macara, R., Swaine, D.J. Fuel, London 1964, 43, 354.
9. Bate, L.C., Nucleonics. 1963, 21, 72.
10. Dibbs, H.P., Department of Mines and Technical Surveys, Mines Branch, Technical Bulletin TB 55, March, 1964.
11. Radmacher, W., Mohrhauer, O., Brennstoff Chem. 1956, 37, 353.

TABLE 1. Results from the determination of oxygen in standards

Standards	Oxygen (%)				
	Determined using				Theoretical
	Pyrolysis method	Mean	Neutron activation method	Mean	
1) Benzoic acid	26.3; 26.7; 26.3; 26.0; 26.5; 26.7; 26.2; 26.3; 26.3;	26.4	26.14; 27.16; 27.12; 25.82; 25.54; 25.71;	26.25	26.20
2) Acetanilide	12.2; 11.7; 12.1;	12.0	12.12; 12.24; 11.76;	12.04	11.84

TABLE 2. Oxygen in coal (the results expressed on the dry coal basis)

Sample	Oxygen (%)				Carbon d.a.f.	Ash
	by pyrolysis method	Mean	by neutron activation method	Mean		
1	2	3	4	5	6	7
<u>Bituminous coals</u>						
Moss 3	6.4; 6.9; 6.4; 7.1; 7.1; 6.9;	6.8	8.17; 8.58; 8.84; 8.60;	8.55	82.4	6.73
Moss 3-demineralized	6.6; 6.6; 6.9;	6.7	6.75; 6.73; 6.13;	6.54		0.29
Itmann	4.2; 4.5; 4.0; 4.0;	4.2	6.40; 6.47; 6.68; 6.58;	6.53	85.1	6.30
Itmann-demineralized	4.3; 4.5; 4.2;	4.3	4.26; 4.24; 4.44;	4.31		0.15
<u>Lignites</u>						
Turow-demineralized	24.9; 26.4; 26.4; 26.5;	26.0	26.13; 26.21; 27.77; 25.99; 25.81;	26.38	68.8	0.25
Smogory-demineralized	29.9; 31.0; 29.8;	30.2	33.75; 32.38; 36.33; 30.77;	31.62	66.3	0.26
<u>Subbituminous coal</u>						
fresh	-	-	24.30; 24.59;	24.43	75.0	6.24
demineralized	-	-	20.00; 20.29;	20.14		0.11
<u>Anthracite</u>						
fresh	1.8; 2.1	2.0	7.59;	7.59	92.5	11.05
demineralized	2.3; 2.0; 2.2;	2.2	2.66;	2.66		0.91

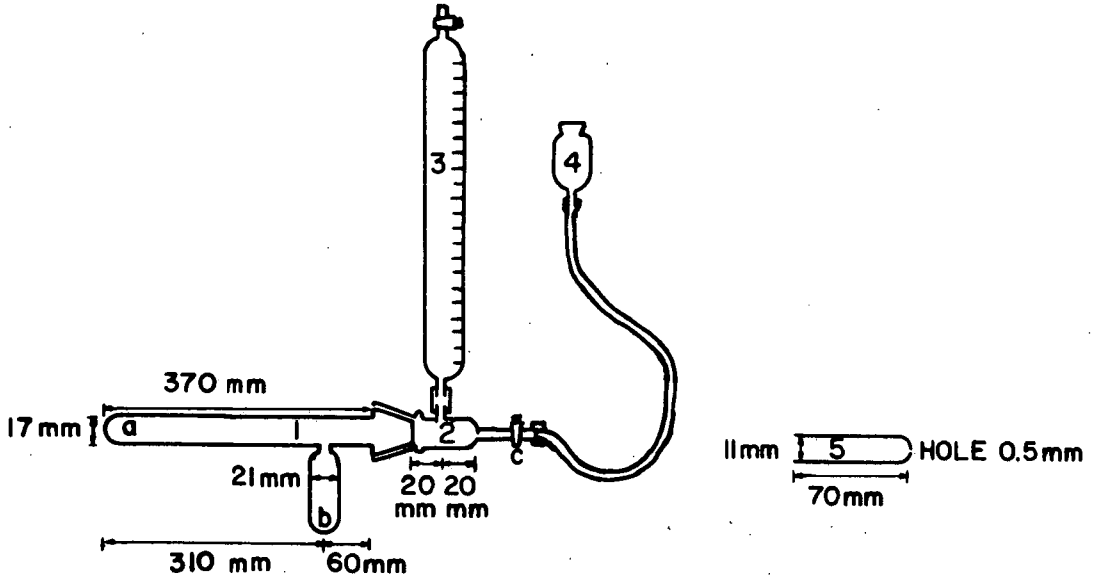


FIGURE 1 - APPARATUS FOR PYROLYSIS CONVERSION AND MEASUREMENT OF VOLUME OF EVOLVED GASES

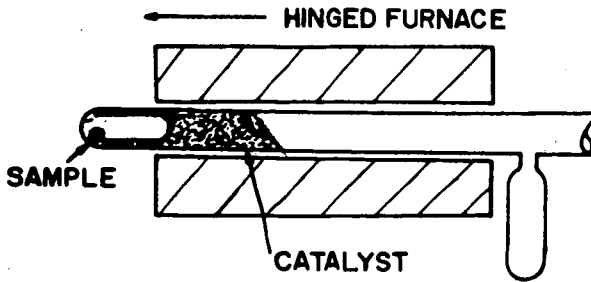


FIGURE 2 - LOCATION OF THE PYROLYSIS TUBING IN OVEN AT THE BEGINING OF EXPERIMENT

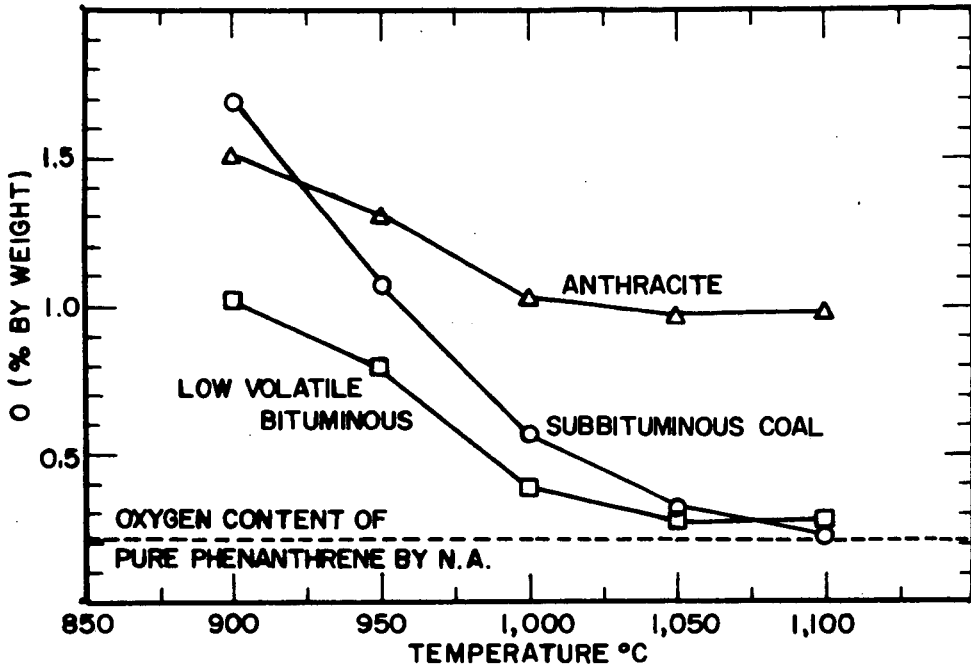


FIGURE 3 - OXYGEN CONTENT BY NEUTRON ACTIVATION OF COKE FROM DEMINERALIZED COAL, PYROLYSED FOR 10 MINUTES AT INDICATED TEMPERATURE

FRACTIONATION OF LOW TEMPERATURE COAL TAR  
BY GEL PERMEATION CHROMATOGRAPHY

Benjamin C. B. Hsieh, R. E. Wood, and L. L. Anderson

Department of Mineral Engineering

University of Utah, Salt Lake City, Utah 84112

Abstract

The use of gel permeation chromatography as a separation tool makes it possible to fractionate coal tar or similar products into three groups of compounds. These are aliphatics, aromatics, and tar acids. The aliphatic hydrocarbons are fractionated as a function of molecular length or carbon number. The aromatic ring compounds are fractionated as a function of molecular size and shape. The effect of adsorption between the polar tar acids and the column support material delays their elution until the other two groups have passed through the column. The elution curves of selected coal tars show the distribution conditions and permit the calculation of percentage composition.

Gel permeation chromatographic data from coal tar distillates (150° to 350°C) were compared to the results of chemical extraction (USBM NaOH-H<sub>2</sub>SO<sub>4</sub> procedure) and the results of FIA (ASTM D-1319 fluorescence indicator adsorption) on the same distillation fraction. A gas chromatograph was used for the qualitative identification of these products. The portion boiling above 350°C also can be analyzed with GPC where chemical extraction, FIA, GC, and mass spectrometric methods are not generally applicable. Because GPC is performed at room temperature, the problems of thermal cracking and polymerization that occur with distillation techniques are avoided.

Introduction

Gel permeation chromatography (GPC) was first mentioned in the literature by Moore in 1964 (1). A comprehensive historical review was published by Cazes (6) in 1966. This technique has since become an accepted method for the determination of molecular weight distribution of polymers and for the fractionation of medium and high molecular weight materials (6). This analytical tool is still somewhat limited to use in the area of polymer sciences and biochemistry. Very few articles have appeared which apply this technique to coal, coal tar, and petroleum products. Hendrickson and Moore (2) first described the elution behavior of aliphatic and aromatic hydrocarbons. Altgelt (3) has studied the molecular weight distribution of asphaltenes by GPC and infrared spectroscopy. Edstrom and Petro (4) reported that aromatic hydrocarbons were fractionated by GPC and also gave elution curves of coal tar pitch and thermal aromatic residues. These authors concluded that separations occur not as a function of a single parameter, but as a complex function of molecular size, shape, and polarity. Their elution curves were correlated with the softening point of the pitch samples with reference to standard aromatic materials. In our laboratory we have applied GPC to the elution

behavior of various kinds of coal tar, crude petroleum, and related materials based on molecular size, shape, and polarity. We have also measured separation characteristics of neutral oils, tar acids, and thermal distillation fractions from coal tar. These were compared to standard aliphatic and aromatic hydrocarbons by means of conventional gas chromatography.

#### Experimental Procedure

The general operation technique for gel permeation chromatography is to dissolve the sample containing materials of different molecular weight in a small volume of solvent. The sample and solvent are introduced at the top of the column. High molecular weight materials pass more rapidly through, while low molecular weight materials pass more slowly due to their diffusion into pores in the beads of the column support materials (5, 6, 7). Chemical affinity of polar materials may act to retard passage of a specific species more than would be expected on the basis of molecular size alone. <sup>1/</sup> Edstrom and Petro (4) first pointed out this effect and it has been verified in our work. The overall effect of the procedure is a separation based on molecular size and shape, but some chemical affinity effects must also be considered.

Tetrahydrofuran (THF) was chosen as the solvent for elution through a Sephadex organic solvent resistant column packed with Sephadex LH-20 beads. The column and support material were supplied by Pharmacia Fine Chemicals, Inc. <sup>2/</sup> The advantages of using THF were pointed out by Hendrickson and Moore (2). A reagent grade tetrahydrofuran from J. T. Baker Chemical Company was used. Its purity was checked by gas chromatography. A small amount of Butylated Hydroxytoluene as stabilizer was added by the manufacturer.

The separation range of Sephadex LH-20 is reported to be from molecular weight 100 to 2000 by the manufacturer (5). A column of approximately 86.5 cm length was operated at room temperature and the solvent was degassed at 55°C before introduction to the column. Samples were introduced by injection with a syringe through a Y-shaped junction with a rubber septum mounted at the head of the column.

The eluted fractions were collected automatically with a Gilson <sup>3/</sup> volumetric fractionator at approximately 10-minute intervals and a flow rate near 0.34 ml per minute. This resulted in 3.40 ml collected for each fraction. Qualitative identification of standard materials passing through the column was

---

<sup>1/</sup> Moore and Hendrickson (7) considered the adsorption and partition effects "are not significant in GPC, since the gel is quite free from associative forces with the sample and is eluted with a solvent having a similar polarity, so that negligible partition of the solute occurs between the gel and solvent phases."

<sup>2/</sup> Pharmacia Fine Chemicals, Inc., 800 Centennial Avenue, Piscataway, N. J. 08854.

<sup>3/</sup> Gilson Medical Electronics, Middleton, Wisconsin.

attained by injection of fractions into an F&M Model 720 gas chromatograph. Apiezon L (4 ft.), silicone grease (2 ft.), and carbowax 20M (8 ft.) columns were used. This unit was programmed from 100° to 300°C at 10 degrees per minute. He carrier gas was used at a flow rate of 100 ml/min.

Quantitative measurement of the amount of sample material collected in each fraction by GPC was done by evaporating the tetrahydrofuran at about 70°C and weighing the residue. Duplicate weighings were reproducible within 0.10 mg on the same fraction residues

Samples of Spring Canyon, Big Horn, and River King coals were selected for study. These coals were carbonized at 550°C. The coal tars from this process were distilled to 150°C. The portions distilling below 150°C were discarded and the portions distilling about 150°C were used as samples. Spring Canyon coal tar was again distilled to give two fractions: 150° to 350°C (distillate) and above 350°C (pitch). The neutral oil and tar acids were chemically separated from the Spring Canyon coal tar distillates by the Bureau of Mines extraction method (8). One other pyrolysis coal tar was studied. This was furnished by Food Machinery Corporation and was examined without further treatment. A petroleum crude oil, a shale oil distillate, and a tar sand benzene extract were fractionated by GPC without prior treatment

### Results and Discussion

Since chemical affinity or absorption between specific materials in the sample and column support beads may affect the physical separation of components, it is important that standard reference materials be measured on the column. Figure 1 is a plot of molecular weight of known reference materials, paraffinic, olefinic, and aromatic hydrocarbons, versus the fraction number where the greatest concentration of each material can be expected to occur. Although each reference material will occur in 4 or 5 adjacent fractions, its greatest concentration, as found by gas chromatography (GC), will occur in the fraction indicated in Figure 1. As shown by this comparison, there is a considerable overlap between aliphatic and aromatic-type compounds. A plot of the data from Hendrickson and Moore (2) where paraffinic and olefinic hydrocarbons and their isomers are all in one group and all aromatic hydrocarbons in another group is in agreement with Figure 1.

The fractions of the Spring Canyon coal tar distillate elution curve, shown in Figure 2, are clearly divided into three groups. The first two groups contain the aliphatic and aromatic hydrocarbons. The third group contains the polar tar acids. Evidence for these statements is found in Figure 3 where elution curves for neutral oil without tar acids and for tar acids alone are shown. The presence of material in the total coal tar distillate, Figure 2, in fractions numbered greater than 85 is attributed to acids and bases that could have an affinity for the Sephadex LH-20. These materials are not found in the sample of neutral oil, Figure 3.

Gas chromatography was used in an effort to more fully understand the GPC separation of coal tar. The fractions collected from GPC were combined into three groups by redissolving the fraction residues in THF. Group I was taken

from fraction number 50 to 66. Group II was taken from fraction number 67 to 85, and group III was taken from fraction number 86 to 125 as indicated in Figure 2. These three portions of the original sample were then analyzed with gas chromatography. A comparison of results from these three composited groups of fractions with standard paraffinic hydrocarbons, aromatic compounds, and tar acids are shown in Figures 4-6. Also, the aromatic compounds were extracted from the same coal tar distillate with pyridine by the method of Qader, et al. (9), for comparison with the composited groups.

The pyridine extraction removes both aromatic and tar acid compounds from the distillate. This is shown by a comparison of Figure 5a (Group II) and Figure 5b (pyridine extract). Removal of the tar acid peaks from Figure 5b shows good agreement between the two. The pattern of Group I shown in Figure 4a compares very well with that from selected standard straight chain paraffinic compounds shown in Figure 4b. The pattern of Group III, Figure 6a, agrees almost exactly with the pattern of tar acids chemically separated from the same distillate, Figure 6b.

In Figures 4-6 peak (1) was identified as the inhibitor from the THF solvent. Although in low concentration in the solvent, its concentration is increased by evaporation of the solvent.

The GC chart of the original coal tar distillate is shown in Figure 7. The total pattern of Figure 7 is the summation of the three separate patterns of Figures 4a, 5a, and 6a. These three group samples were analyzed with an Apiezon L column and also with Silicone Grease and Carbowax 20M columns. Different known standard paraffins, aromatics, and phenols were added to these three samples separately. Some peaks were matched and identified as paraffins, aromatics, and phenols in the three composited fraction portions of the original sample, respectively.

Using GPC, it is possible to separate coal tar products into aliphatic and aromatic fractions by molecular shape. Tar acids are separated into a third fraction by chemical affinity with the GPC column support material. This separation is as precise and accurate as the standard chemical methods which are used for coal tar analysis (8, 10, 11).

The fundamental separation of GPC is determined by molecular size. Figure 8 shows a comparison of two distillation fractions from a low temperature coal tar sample. The solid line represents the chromatogram obtained from the 150° to 350°C fraction, distillates, and the dotted line that from the 350° to 550°C fraction, pitch. These curves show that in the pitch or high boiling material, the paraffinic group and the aromatic group are both distributed toward the lower fraction numbers. In the low boiling distillates the two groups are distributed toward the higher fraction numbers. This indicates that the pitch portion contains compounds of greater molecular size than does the distillates portion, as would be expected. The summation of these two curves gives the total coal tar distribution curve almost identical to that of the original material shown in Figure 9c.

The pattern of the distillate portion, Figure 2, begins with fraction number 50. From this we infer (Figure 1) that the highest molecular weight paraffinic

compound in the distillate is C<sub>31</sub>. This is in agreement with the GC data. Although we can find C<sub>32</sub> and C<sub>33</sub> peaks on the GC pattern, they are very small compared to the C<sub>30</sub> and C<sub>31</sub> peaks. At the low temperature boundary of the distillate range (150°C), the smallest paraffinic number possible is C<sub>9</sub> (boiling point 150.8°C). This is also in agreement with the GC pattern, Figure 7, where C<sub>9</sub> is the first peak indicated. Termination of Group I at fraction number 66 would suggest, from Figure 1, that C<sub>11</sub> paraffins could be included. However, the paraffins C<sub>9</sub> to C<sub>11</sub> are easily vaporized and may be lost in the solvent evaporation step. As a result, C<sub>12</sub> is the lowest boiling compound found in Group I by GC, Figure 4a.

It is important that the coal tar components that boil below 150°C be removed prior to GPC. The aliphatic materials that boil in this range, primarily components of the conventional "gasoline cut," may overlap into the aromatic portion of the GPC curve. The lower boiling aromatic components, such as benzene, xylene, and toluene which are also removed by this process, do not overlap into the tar acid portion of the GPC curve. The GC patterns of Groups II and III show no evidence of overlapping materials (Figures 5a and 6a).

GC peaks of Group I, Figure 4a, are produced by paraffinic hydrocarbons. Although olefinic compounds may be present, they are low in concentration (2-3%) as shown by FIA tests and are not registered in Figure 4a. The absence of aromatics in group I is evidence that aromatic compounds of high ring number (over 4) are not present in coal tar. If present, these high-boiling materials would elute with the C<sub>9</sub>-C<sub>12</sub> aliphatic hydrocarbons. The lack of high ring number aromatics is to be expected since low temperature carbonization (550°C) should produce only those coal tar components with boiling point below this temperature. The most significant aromatic materials (Figure 5) are those boiling in the naphthalene to anthracene range (218° to 354°C).

Again, reference to Figure 1 shows a different slope or separation factor for homologous aromatic compounds of different size or configuration. The slope of the curve propyl benzene, ethyl benzene, and toluene was plotted from the data of Hendrickson and Moore (2). The slopes of the two curves (a) 2 methyl anthracene, 2 methyl naphthalene, and toluene, and (b) biphenyl, terphenyl, quaterphenyl, etc., are plotted from the data of Edstrom and Petro (4). All the data were transposed to our reference scales based on the slope of the benzene, naphthalene, anthracene, and naphthacene curve. From these four curves we infer that a simple curvilinear function does not describe the GPC separation characteristic for aromatic compounds. Therefore, in Group II, we do not find an orderly distribution of components by number of rings or any other single parameter.

The distribution curves of coal tars from some representative coal types are shown in Figure 9. The chemical characteristics of these coals are listed in Table 1. All these coals were carbonized at 550°C and the fraction boiling below 150°C removed prior to separation by GPC. Figure 10 shows the GPC curves for a crude petroleum, a shale oil, and a tar sand extract.

Table 2 contains the percentages of aliphatics, aromatics, and tar acids found in the samples of Figures 9 and 10. Coal tars from the low temperature

carbonization of three coals (Big Horn, River King, and Spring Canyon), a petroleum crude (Red Wash), a shale oil distillate from Rifle, Colorado, a tar sand extract from the Utah Geological Survey, and a pyrolysis low temperature tar (FMC) were included. Also included in Table 2 are GPC data for products from Spring Canyon coal tar. Pitch (B.P. 350° to 550°C), duplicate measurements on distillates (B.P. 150° to 350°C), and neutral oil from the distillate fraction are shown. A chemical measurement of the tar acids in the distillate sample and an FIA (10) measurement of the aliphatics and aromatics in the neutral oil sample are also shown. The weights of residues in fractions 1-66 (aliphatics), 67-85 (aromatics), and 86 to 125 (tar acids) were used in the calculation of percentage composition. The figures in parentheses represent the calculated percentages of aliphatics and aromatics in the neutral oil; that is, the product following removal of tar acids and bases from each sample.

Spring Canyon coal, which is a high volatile bituminous coal, was used for most of our determinations. The percentages of aliphatics and aromatics in the total coal tar from this coal are about the same. The tar acids percentage in the total coal tar is less than that reported from the distillates. This means that the tar acids are distributed toward the lower boiling point (or low molecular weight) compounds. In pitch, the opposite is true. The tar acids percentage is lower than in the total coal tar and aliphatic compounds are predominant. Another high volatile bituminous coal used in this study was River King, which contains 3.30 percent sulfur. The GPC elution curve indicates that this coal tar contains a high percentage of aromatic and tar acid compounds and a relatively low percentage of aliphatic hydrocarbons. Coal tar from a subbituminous coal, Big Horn, is little different from coal tar from Spring Canyon coal. However, this low rank coal (17.2% O<sub>2</sub>), when carbonized, did produce more water and somewhat more acids than did the Spring Canyon coal.

The three low temperature coal tars studied show very little weight percent in fractions numbered less than 50. This is an indication that aliphatic hydrocarbons of length C<sub>40</sub> and higher are not produced in the low temperature carbonization process at 550°C. However, the GPC curve from a pyrolysis coal tar (FMC), also shown in Figure 9, does show a significant weight percent in fractions numbered less than 50. This curve indicates a predominantly aliphatic content rather than aromatic or tar acid composition. This is due to the fact that this material was pyrolyzed at a temperature of 870°C.

Shale oil distillates, petroleum crude oil, and benzene extractants from a tar sand sample, Figure 10, show high percentages of aliphatic hydrocarbons. The increased proportion of high carbon number paraffins can be seen in the higher weight percent in fractions numbered less than 50

### Conclusions

The results of this investigation show that GPC is a useful tool for the study of distribution of coal-derived liquids. These liquids may come from carbonization coal tars, hydrogenation or hydrocracking products, or solvent extracted products, etc. Similar composition materials such as petroleum

crude and its products, shale oil, gilsonite, and tar sand extractants, etc., can also be fractionated. GPC readily fractionates these samples into three groups, aliphatics, aromatics, and tar acids, based on the factors of molecular size, shape, and polarity. This procedure is specifically interesting because it is capable of making separations of these high boiling, high molecular weight materials at room temperature. The problems of thermal cracking and polymerization when distillation is used for fractionation are minimized. High boiling pitches and tars that cannot be analyzed with gas chromatography, mass spectrometry, the ASTM FIA or the USBM chemical extraction method can be fractionated with this procedure.

#### Acknowledgement

The research work reported in this paper is sponsored by the U. S. Office of Coal Research and the University of Utah.

Table I. Proximate and ultimate analysis of selected coals

	Spring Canyon H.V. bituminous		Big Horn subbituminous		River King H.V. bituminous	
V.M.	47.60	(53.10)	38.80	(46.49)	38.64	(48.26)
Moisture	1.90	Free	14.30	Free	8.26	Free
Ash	8.46	Free	2.22	Free	11.68	Free
F.C.	42.04	(46.90)	44.68	(53.51)	41.42	(51.74)
S	0.46		0.60		3.30	
O	9.67		17.21		9.61	
C	71.10		62.40		62.40	
N	1.40		0.70		1.40	
H	5.10		4.10		4.20	

Table II. Percentage results from GPC fractionation method.

Sample	I	II	III
	aliphatics 0-66	aromatics 67-85	tar acids 86-125
Red Wash (Crude oil)	82.21% (87.89%)*	11.33% (12.11%)*	6.46%
Tar sand (Benzene extractants)	69.10% (79.30%)	18.04% (20.70%)	12.86%
Shale oil (Distillate from Rifle, Colorado)	68.24% (83.21%)	17.77% (16.79%)	13.99%
F.M.C. (Pyrolysis coal tar)	57.71% (67.89%)	27.30% (32.11%)	14.99%
Spring Canyon (High volatile bituminous coal)	37.22% (47.98%)	40.36% (52.02%)	22.42%
Big Horn (Subbituminous coal, 17.2% O <sub>2</sub> )	31.21% (44.80%)	38.45% (55.20%)	30.34%
River King (High volatile bituminous coal, 3.30% S)	18.37% (29.71%)	43.47% (70.29%)	38.16%
Pitch (From Spring Canyon coal tar)	47.07% (58.87%)	32.88% (41.13%)	20.05%
Neutral oil (From Spring Canyon coal tar distillate)	42.60% (41.77%)	57.40% (58.23%)	
Tar acids from Spring Canyon coal tar by chemical method			34-36%
Neutral oil from Spring Canyon coal tar by FIA method	(38-42%)	(58-62%)	
Distillates (1) from Spring Canyon coal tar (150°-350°C)	24.09% (38.28%)	38.03% (60.43%)	37.88%
Distillates (2) from Spring Canyon coal tar (150°-350°C)	22.62% (36.72%)	38.98% (63.27%)	38.40%

\* The percentages of aliphatics and aromatics in the neutral oil where tar acids and tar bases have been removed are indicated by the use of parentheses.

Literature Cited

1. Moore, J. C., J. Polymer Sci., Part A, 2, 835-843 (1964), "Gel Permeation Chromatography, I. A New Method for Molecular Weight Distribution of High Polymers"
2. Hendrickson, J. G., and Moore, J. C., J. Polymer Sci., Part A-1, 4, 167-188 (1966), "Gel Permeation Chromatography, III. Molecular Shape versus Elution"
3. Altgelt, K. H., J. of Applied Polymer Sci., 9, 3389-3393 (1965), "Fractionation of Asphaltenes by Gel Permeation Chromatography"
4. Edstrom, T., and Petro, B. A., ACS Chicago meeting, Sept. 1967, "Gel Permeation Chromatographic Studies of Polynuclear Aromatic Hydrocarbon Materials"
5. Sephadex gel filtration in theory and practice, Pharmacia Fine Chemicals, Inc., 1967
6. Cazes, J., J. of Chemical Education, 43, A 567-582 (1966), "Gel Permeation Chromatography, Part One," 43, A625-642 (1966), "G.P.C., Part Two"
7. Moore, J. C., and Hendrickson, J. G., J. of Polymer Sci., Part C, 8, 233-241 (1965), "Gel Permeation Chromatography II. The Nature of the Separation"
8. Fisher, C. H., and Eisner, A., Industrial and Eng. Chem. Analytical Edition, 9, 213-218 (1937), "Determination of Tar Acids and Bases by Extraction Methods"
9. Qader, S. A., et al., India Patent No. 94932, Oct 29, 1966
10. ASTM, D1319, Hydrocarbon Types in Liquid Petroleum Products (FIA Method)
11. Standard Methods for Testing Tar and its Products, Fifth Edition (1962), published by the Standardization of Tar Products Tests Committee, printed in Great Britain, W. Heffer & Sons Ltd., Cambridge, England

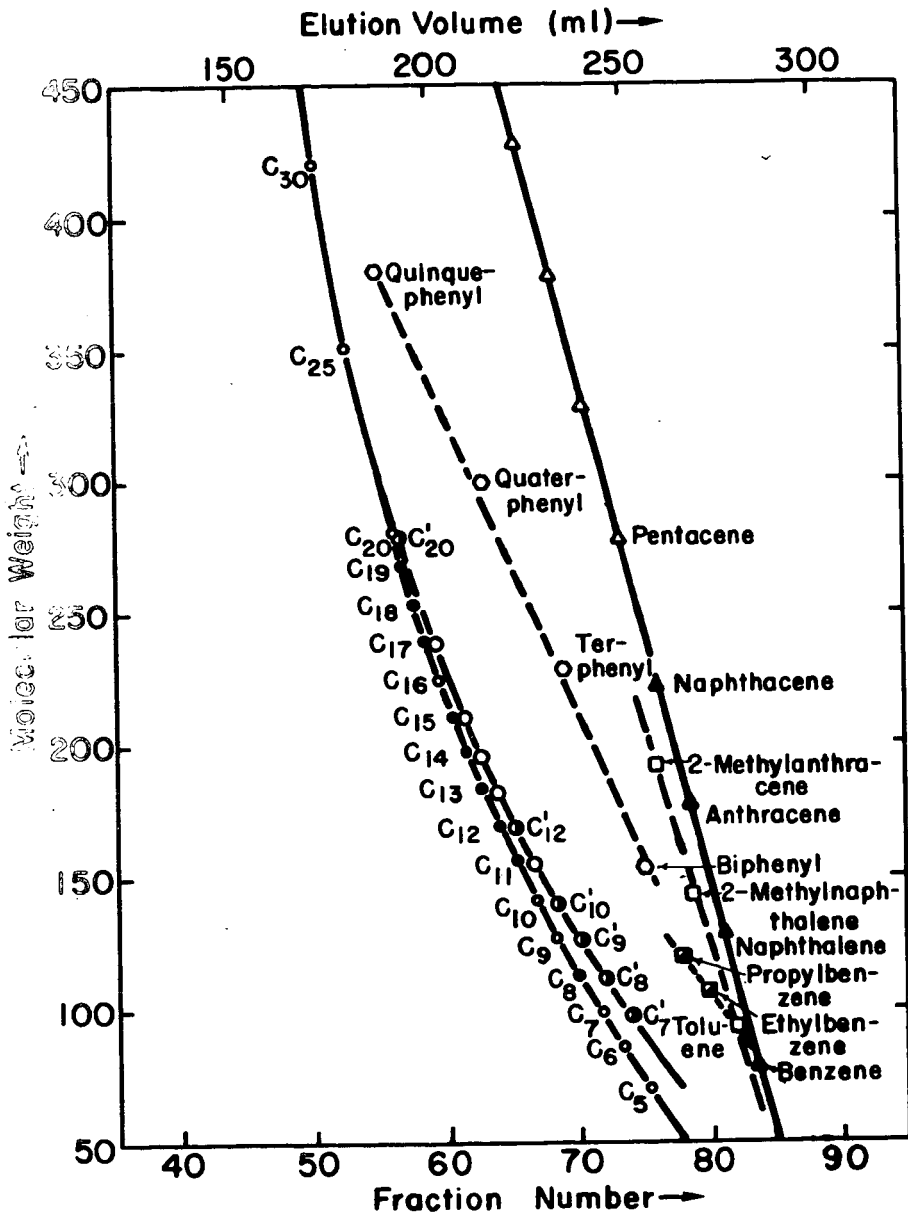


Figure I. GP Chromatography of known hydrocarbons: paraffins, olefins, and aromatics.

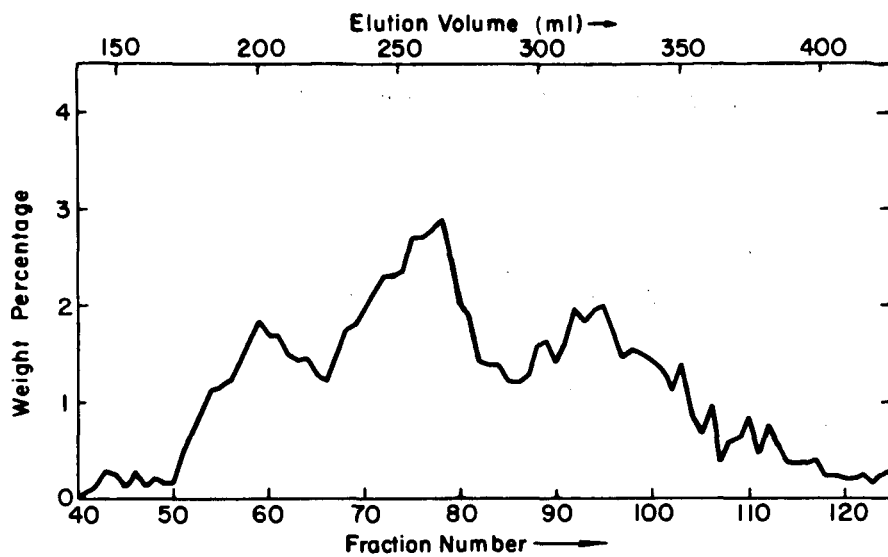


Figure 2. Elution curves (GPC) of low temperature coal tar distillates (150°–350°C) from Spring Canyon coal.

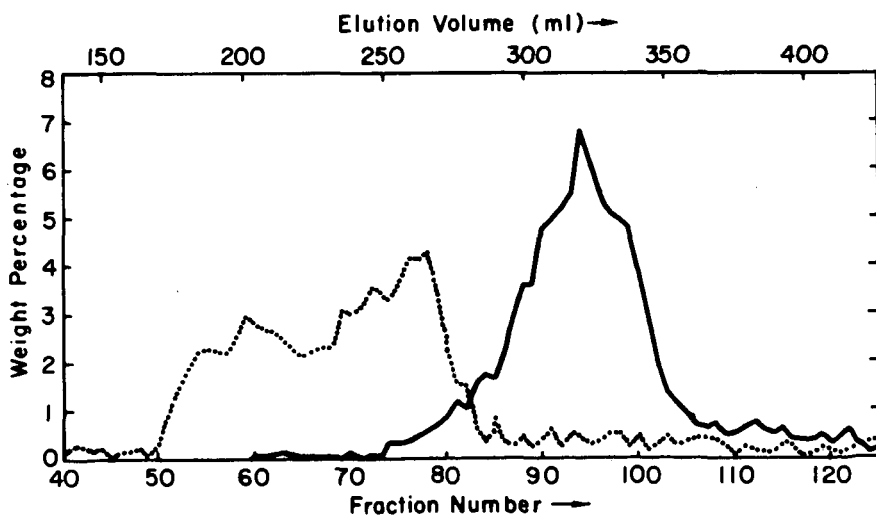


Figure 3. Elution curves (GPC) of neutral oil and tar acids from Spring Canyon coal tar distillates (150°–350°C).

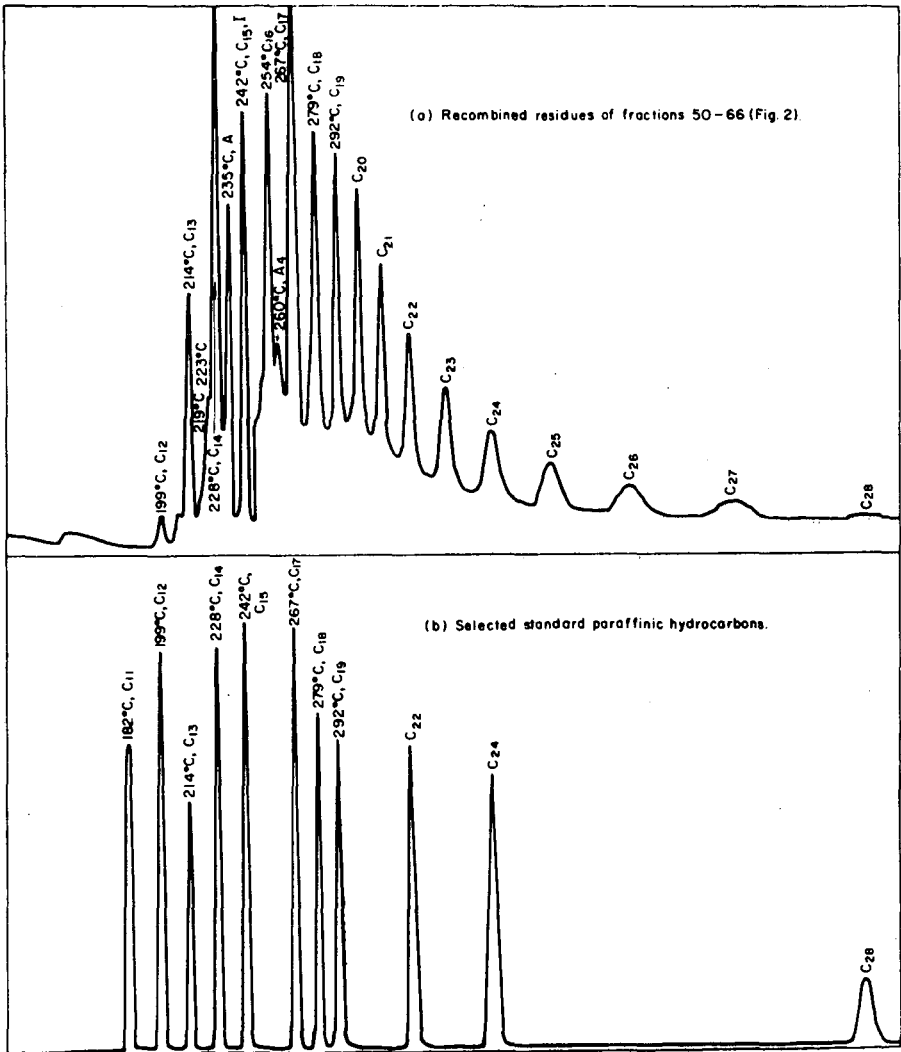


Figure 4. GC Chromatograms.

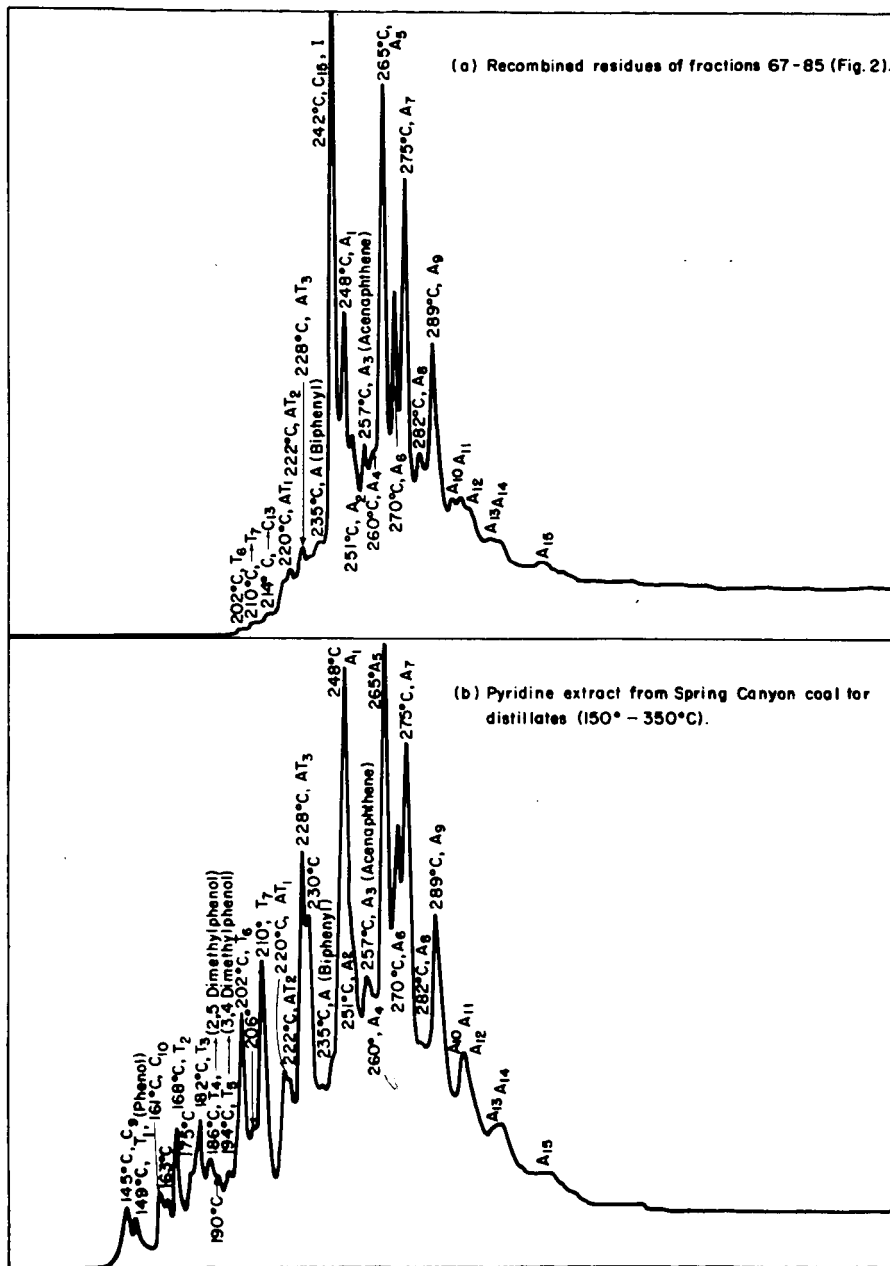
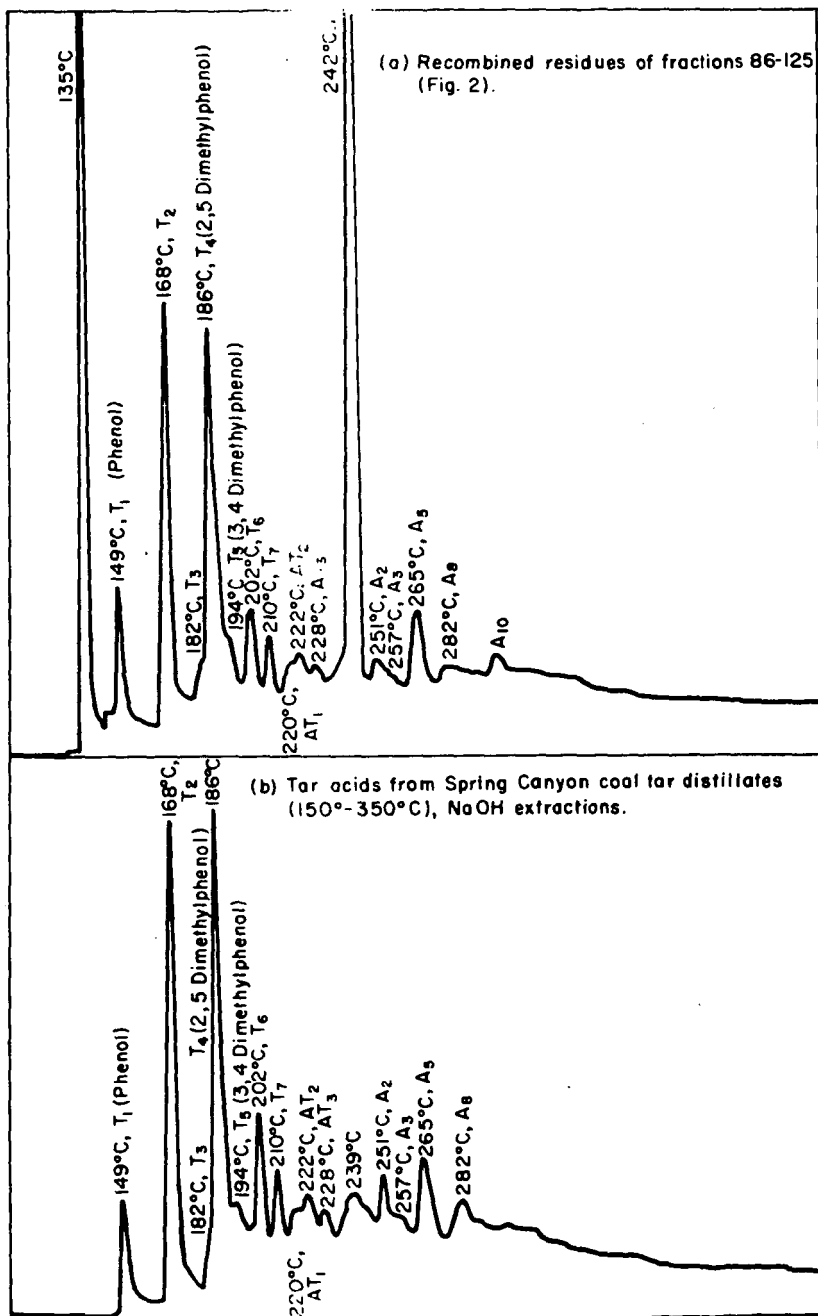


Figure 5. GC Chromatograms



DSC thermograms.



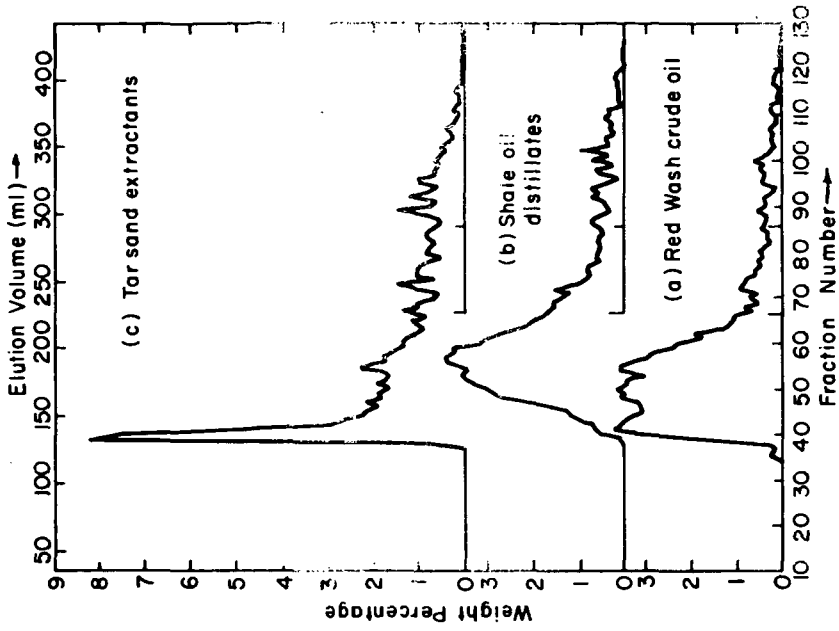


Figure 10. GPC elution curves.

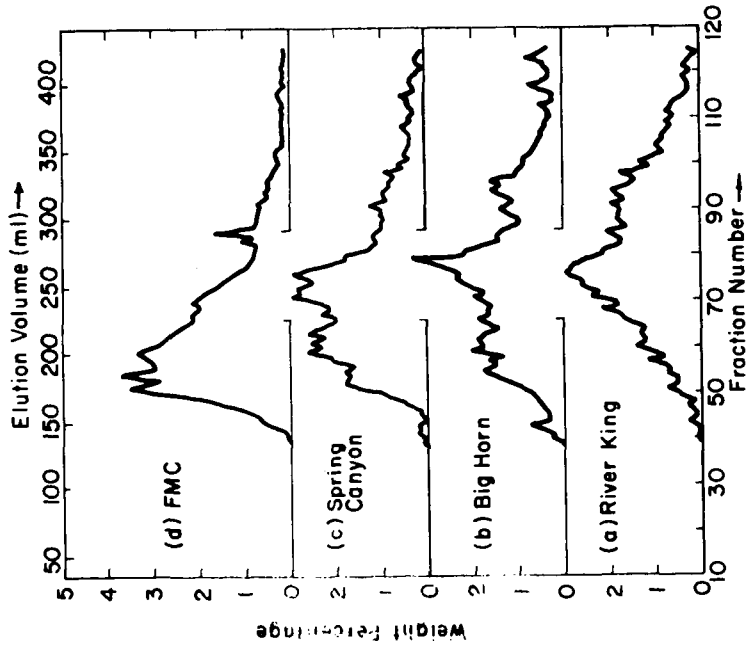


Figure 9. GPC elution curves.

(a) River King coal tar (150°-550°C)

(b) Big Horn coal tar (150°-550°C).

(c) Spring Canyon coal tar (150°-550°C.)

(d) Food Machinery Corporation pyrolysis coal tar.

## SILYLATION OF ASPHALTS WITHIN GLC COLUMNS. EFFECTS ON INVERSE GLC DATA AND INFRARED SPECTRA

S. M. Dorrence and J. C. Petersen

Laramie Petroleum Research Center, Bureau of Mines  
U. S. Department of the Interior, Laramie, Wyoming

### INTRODUCTION

Inverse gas-liquid chromatography (IGLC) has indicated differences in the chemical composition of whole asphalts (1-4) as well as fractions from asphalts (1, 5). IGLC measures interactions between the functional groups of volatile test compounds and functional groups in the liquid phase, which in our studies is asphalt. The asphalt may be analyzed either as-received or after an in-column oxidation procedure.

Asphalt contains many types of functional groups that may exhibit selective affinity for specific test compounds. The identification of selective interactions between functional groups of asphalts and test compounds would provide interpretive information about IGLC data and its relation to the chemical composition of asphalts. Such information is important because previous work has established empirical correlations between IGLC data for specific test compounds and in-use performance (4) or accelerated weathering durability (2, 3).

One approach to the identification of IGLC interactions is selective blocking of functional groups in the asphalt. Work with other materials has shown that silylating reagents are reactive toward certain functional groups containing active hydrogens. Such groups are known to be present in asphalts. These active hydrogen groups are believed to interact strongly with certain test compounds used in IGLC. In the present study N,O-bis(trimethylsilyl)acetamide (BSA) was used to silylate these groups in asphalts. Using a novel approach, silylation is conveniently carried out *in situ* by injecting BSA directly into the IGLC column. Independent work published after completion of this study made use of in-column silylation of volatile solutes (6).

In the present study, IGLC data were obtained on a number of oxidized and unoxidized asphalts that had been silylated. These data are compared with data from samples before silylation.

Infrared spectra were obtained on asphalts recovered from the columns. These spectra are correlated with IGLC data to provide information about functional group interactions between test compounds and asphalts.

### EXPERIMENTAL

#### Apparatus and Procedure

IGLC data were obtained on a Beckman GC-2A gas chromatograph.\* Columns were prepared using  $\frac{1}{8}$ -inch by 12 $\frac{1}{2}$ -foot aluminum tubing packed with 1 part asphalt on 10 parts by weight of 20-40 mesh Fluoropak 80. Columns were conditioned at 130°C for at least 6 hours, using a helium inlet gauge pressure of 15 psi. Following conditioning, test compounds (0.1  $\mu$ l) were then

---

\*Mention of specific products or brand names is made for information only and does not imply endorsement by the Bureau of Mines.

introduced separately and retention times determined. In this study, two columns were prepared from each asphalt. One column was used to obtain test compound retention data on the original asphalt followed by in-column silylation after which retention data were again obtained. The second column was oxidized by the introduction of air under conditions previously reported (2, 3), and retention data were obtained. This was followed by in-column silylation, and retention data were again obtained.

Silylation. - The in-column silylation of asphalt samples was performed in a manner similar to that used to treat column packing supports to prevent "tailing of peaks" from polar materials (7-10). The column to be treated was heated to 160° C while blanketing with helium carrier gas. Four portions of BSA were then injected at 30-minute intervals, the first portion being 200  $\mu$ l and the remainder being 100- $\mu$ l quantities. One hour after injection of the final portion, the temperature was lowered to 130° C and held overnight (at least 15 hours) to elute excess BSA and reaction by-products. Inverse GLC data were then obtained.

Infrared Spectra. - Infrared spectra were obtained with a Perkin-Elmer Model 521 double-beam spectrophotometer using solvent compensation. Asphalt samples were recovered from the IGLC packing for infrared study with  $\text{CCl}_4$  using a modified Soxhlet extraction. The solution obtained was adjusted so that the asphalt concentration was 20g/l. The spectra were obtained on these solutions using 1 cm sodium chloride cells.

Materials. - N,O-Bis(trimethylsilyl)acetamide (BSA) and hexamethyldisilazane (HMDS) were used as received from Pierce Chemical Company. Wilmington (Calif.) asphalt (11) and two asphalts, D and J, from the Zaca-Wigmore Experimental Road Test (12) were used in this study. The former was prepared in this laboratory, and the latter two were furnished by the Materials Division of the Bureau of Public Roads.

#### Calculation of the Specific Interaction Coefficient ( $I_g$ )

Specific interaction coefficients for the test compounds were calculated according to the following equation:

$$I_g = 100 [\log V_g (\text{test compound}) - \log V_g (\text{hypothetical n-paraffin})].$$

$I_g$  is different from the interaction coefficient ( $I_p$ ) used in earlier work (1) in that specific retention volume ( $V_g$ ) rather than corrected retention volume ( $V_R^0$ ) is used in the calculations. The specific interaction coefficient thus obtained is a measure of interactions between the chemical functionalities of the asphalt and the test compound.

## RESULTS AND DISCUSSION

### Effect of Silylation on Inverse GLC Retention Data

Treatment of an inverse GLC column at 160° C with either HMDS or BSA resulted in a rapid reaction. By observing changes in the IR spectra of recovered asphalts following silylation, BSA was found to be more reactive than HMDS and, therefore, was chosen for further studies. Attempts to silylate asphalt samples in solution, using either BSA or HMDS, were unsuccessful because of slow reaction due to low boiling points of the solvents.

Data in Table I show that the specific interaction coefficients for phenol and propionic acid decrease on silylation. The interaction coefficients for acidic test compounds, particularly phenol, have been shown to correlate with service performance in both accelerated weathering and road test studies (2-4). Values of the  $I_g$  on all asphalts (oxidized or not) fall into narrow ranges for both test compounds after silylation. The range for phenol on silylated, as-received asphalts is 112 to 117; that for silylated-oxidized asphalts is 113 to 117. Ranges for propionic acid were 65 to 67 and 69 to 71, respectively. As a net result, all of the silylated asphalts are indistinguishable by these two test compounds. These data indicate that certain functional groups

TABLE I. - Comparison of specific interaction coefficients for asphalts, oxidized asphalts, and trimethylsilyl derivatives of both

Test compound	Asphalt sample <sup>a</sup>	Specific interaction coefficients (I <sub>g</sub> )											
		W	WS	WO	WOS	D	DS	DO	DOS	J	JS	JO	JOS
Phenol		129	112	161	113	136 134	116 113	154 155	117 115	120	117	160	115
Propionic acid		94	67	108	71	97 --- <sup>b</sup>	65 65	154 157	71 69	72	65	99	71
Formamide		150	142	172	165	155 157	--- <sup>b</sup> 150	188 187	183 185	126	128	155	153

<sup>a</sup> W, D, and J refer to Wilmington (Calif.) asphalt, asphalt D and asphalt J, respectively. S designates a sample silylated with BSA, and O designates a column-oxidized sample. Separate determinations on different samples of asphalt D are shown.

<sup>b</sup> This value was not obtained.

that form on oxidation and interact strongly with phenol and propionic acid are blocked by silylation. Silylation also appears to block a portion of the strongly interacting groups present in as-received asphalts.

Phenols and carboxylic acids are compound types present in asphalts. These compound types contain active hydrogens and are believed to interact strongly with the test compounds phenol and propionic acid in IGLC columns via hydrogen bonding. Silylating reagents such as BSA form ethers and esters with phenols and carboxylic acids, respectively, thus reducing their ability to hydrogen bond. Therefore, it is concluded that the phenolic and carboxylic acid OH groups in asphalts are silylated by the technique used in this study, thus strongly suggesting that decreases in the  $I_g$  values for the test compounds phenol and propionic acid result from silylation of these groups.

Data in Table I show that even though the  $I_g$  values for phenol and propionic acid after silylation have narrow ranges the values are still high. These high, relatively constant values indicate that the silylated asphalt samples contain approximately the same concentration of other types of functional groups that interact with phenol or propionic acid.

The formamide  $I_g$  values (Table I) for oxidized or silylated-oxidized asphalts are in the same range (155 to 188, compared to 153 to 185). Ranges for as-received and silylated asphalts are also comparable, these being 127 to 157 and 128 to 150, respectively. Because the specific interaction coefficients for formamide decrease only slightly on silylation, it appears that formamide does not interact appreciably with groups that can be silylated. The carbonyl group is a major type of functional group formed on oxidation (13) that is not silylated with BSA by the current technique. Carbonyl groups have been shown (14) to interact strongly with formamide in GLC determinations. Because oxidized asphalts (whether silylated or not) have higher  $I_g$  values than corresponding unoxidized samples, and because carbonyl groups are polar functions formed on oxidation which are not silylated, it is concluded that carbonyl groups contribute appreciably to  $I_g$  values for formamide.

#### Effect of Silylation on Infrared Spectra

Infrared spectra of dilute solutions of trimethylsilylacetamide, a silylated asphalt, and an asphalt are shown in Figure 1. The infrared band at  $3610\text{ cm}^{-1}$  has been assigned to the free phenolic OH stretching band (15). Based on work in this laboratory, the band at  $3540\text{ cm}^{-1}$  has been assigned to the free carboxylic acid OH stretching band. The band at  $3420\text{ cm}^{-1}$  is attributed to the free amide NH stretching band of trimethylsilylacetamide. The latter assignment was made on the basis of trapping the effluent from silylation reactions and comparing its infrared spectrum with that of trimethylsilylacetamide obtained by hydrolysis of BSA. These spectra were essentially identical. The band at  $3420\text{ cm}^{-1}$  appeared within the known range for NH stretching of amides. The infrared spectrum for BSA has no such band.

The infrared spectra of silylated asphalts show that silylation significantly decreases the absorbance in the  $3610$  and  $3540\text{ cm}^{-1}$  regions. Little, if any, trimethylsilylacetamide remains in the asphalt sample after silylation. This is demonstrated by the absence of a sharp band in the silylated asphalt spectrum in the  $3420\text{ cm}^{-1}$  region. The infrared data are summarized in Table II. In all cases, decreases in absorbances for free phenolic and carboxylic acid OH groups are evident after silylation, indicating that most of these groups react with BSA. Previous discussion of IGLC data concluded that silylation blocks phenolic and carboxylic acid OH groups in asphalt and that these groups probably interact strongly with phenol and propionic acid in IGLC columns. The infrared spectra show that free phenolic and carboxylic acid OH groups are essentially eliminated by silylation.

When free carboxylic acid and phenolic OH absorbance values for as-received asphalts are compared with values for oxidized asphalts, decreases in absorbance values for Wilmington

TABLE II. Comparison of infrared spectra of asphalt samples

Sample <sup>b</sup>	Absorbance <sup>a</sup>	
	Free phenolic OH, 3610 cm <sup>-1</sup>	Free carboxylic OH, 3540 cm <sup>-1</sup>
W	0.130	0.045
WS	<0.005 <sup>c</sup>	<0.005
D	0.097	0.028
DS	0.019	<0.005
J	0.035	0.020
JS	0.009	0.006
-----		
WO	0.070	0.028
WOS	<0.005	<0.005
DO	0.111	0.034
DOS	0.017	<0.005
JO	0.015	0.009
JOS	0.006	<0.005

<sup>a</sup>The values given are for 20g/l solutions of the sample in CCl<sub>4</sub> using 1 cm cells without solvent compensation. They were determined by the base-line technique.

<sup>b</sup>See footnote from Table I for sample designation

<sup>c</sup>The lower limit of detectability was about 0.005 absorbance units.

asphalt and asphalt J are observed. These results seem contradictory to the conclusion that increased concentrations of phenolic and carboxylic acid OH groups relate to the increase in  $I_g$  values for phenol and propionic acid. However, it has been shown previously (15) that column oxidation of asphalts results in a decrease of free OH absorbance while hydrogen-bonded OH absorbance increases significantly. Much of this hydrogen bonding remains intact even in dilute solutions so that the net result is a loss of free OH absorbance even though the total OH in the sample has increased. Upon silylation a general decrease is noted in the hydrogen-bonded absorbance; however, no quantitative determination could be made of the hydrogen-bonded region (about  $3500-2500\text{ cm}^{-1}$ ) because it is overlapped by the C-H stretching region.

#### Repeatability of the Silylation Technique

Two separate packings were prepared, using asphalt D as the substrate. Two columns of each packing were processed in the manner described in the Experimental section. The data, included in Table I, show a maximum variation in specific interaction coefficients for a given test compound on duplicate asphalt samples of three  $I_g$  units. This is within the normal variation on duplicate runs of the same sample. The preliminary indication is that the technique gives reproducible results.

### SUMMARY AND CONCLUSIONS

Silylation of an asphalt within an IGLC column offers a convenient means to study asphalt functionality. More specifically, the reagent, BSA, reacts with most of the phenolic and carboxylic acid hydroxyl groups present in either as-received or column-oxidized asphalts. Comparison of infrared spectra before and after silylation substantiates this conclusion.

Silylation reduces the phenol and propionic acid  $I_g$  values on both oxidized and unoxidized asphalts to a common value characteristic for each individual test compound. This results from the blocking of the carboxylic acid and phenolic OH groups in the asphalts. These groups are believed to be the ones by which phenol and propionic acid differentiate among asphalts. The functional groups which interact strongly with formamide remain after silylation. These groups appear to be carbonyl functions.

The silylation technique should be applicable to investigations of the chemical structure of macromolecules and nonvolatile materials.

### ACKNOWLEDGMENTS

Technical discussions with Dr. George Bohner of the Denver Research Institute are gratefully acknowledged.

Work presented in this paper was done under a cooperative agreement between the Bureau of Mines, U.S. Department of the Interior and the University of Wyoming.

### LITERATURE CITED

1. T. C. Davis, J. C. Petersen, and W. E. Haines, *Anal. Chem.*, **38**, 241 (1966).
2. T. C. Davis and J. C. Petersen, Highway Res. Rec. No. 134, Highway Research Board, National Research Council, 1 (1966).
3. T. C. Davis and J. C. Petersen, *Anal. Chem.*, **38**, 1938 (1966).
4. T. C. Davis and J. C. Petersen, *Proc. Assoc. Asphalt Paving Technologists*, **36**, 1 (1967).
5. T. C. Davis and J. C. Petersen, *Anal. Chem.*, **39**, 1852 (1967).
6. G. G. Esposito, *Ibid.*, **40**, 1902 (1968).

7. J. Bohemen, S. H. Langer, R. H. Perrett, and J. H. Purnell, *J. Chem. Soc.*, 1960, 2444.
8. D. T. Sawyer and J. K. Barr, *Anal. Chem.*, 34, 1518 (1962).
9. R. H. Perrett and J. H. Purnell, *J. Chromatog.*, 7, 455 (1962).
10. R. A. Dewar and V. E. Maier, *Ibid.*, 11, 295 (1963).
11. W. E. Haines, *Proc. Amer. Petrol. Inst.*, Sect. VIII, 42 (8) 51 (1962).
12. F. N. Hveem, E. Zube, and J. Skog, *ASTM Special Technical Publication No. 277*, 3 (1959)
13. P. G. Campbell and J. R. Wright, *J. Res. Nat. Bur. Stand.*, 68C, 115 (1964).
14. J. Novák and J. Janák, *Anal. Chem.*, 38, 265 (1966).
15. J. C. Petersen, *Fuel*, 46, 295 (1967).

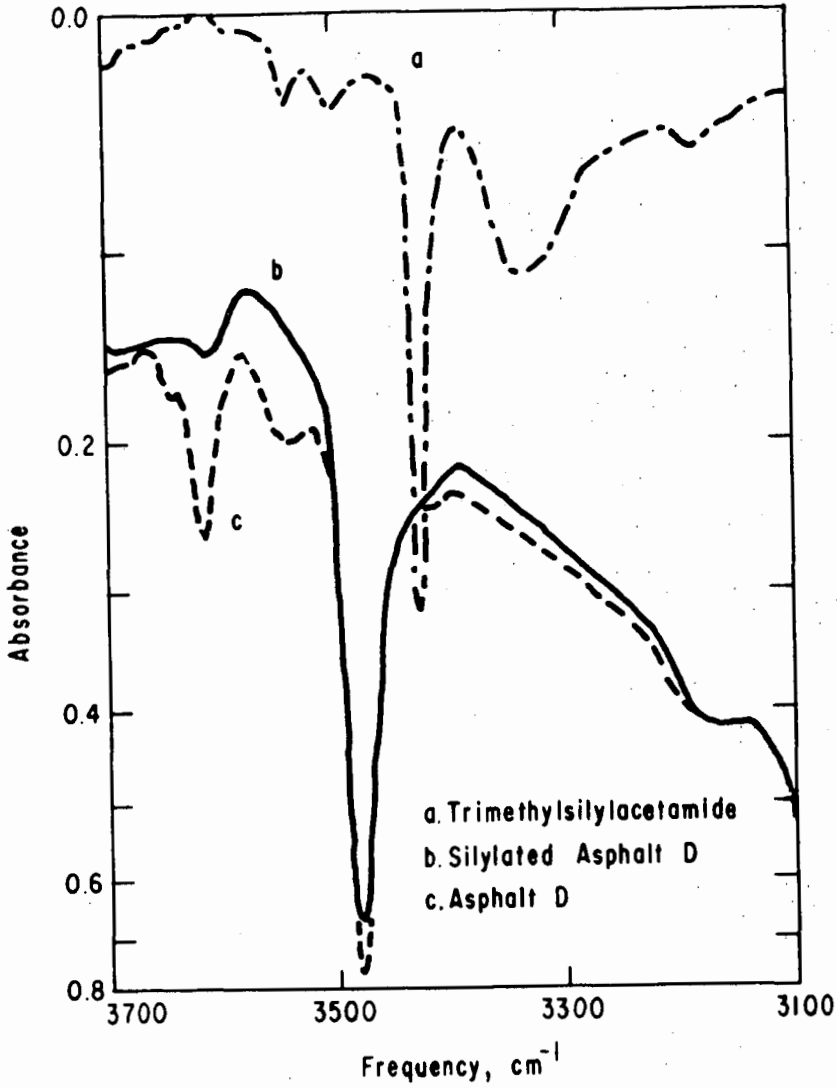


Figure 1. Infrared Spectra of Trimethylsilylacetamide, Silylated Asphalt D, and Asphalt D

KINETICS OF HYDRAZINIUM DIPERCHLORATE THERMAL  
DECOMPOSITION BY FLASH MASS THERMAL ANALYSIS\*

J. A. Hammond, Yuji A. Tajima, W. Glenn Stapleton, W. E. Baumgartner

Lockheed Propulsion Company, Redlands, California

## 1. INTRODUCTION

The kinetic mechanisms of decomposition of propellant ingredients are of vital interest to the propellant chemist when it becomes necessary to forecast propellant thermal stability and shelflife, to determine the ignition and combustion kinetics of the propellant, and to predict the sensitivity of the propellant to impact (shock) or frictional forces. In each case, the energetics and mechanism of the initiation step, and the products formed thereby are important. These parameters are not easily obtained by most experimental techniques for measuring reaction kinetics.

## 2. BACKGROUND

Unique techniques for determining the energetics and kinetics of the initiating reaction which occur during pyrolysis of solid propellant ingredients have been developed. These techniques involve the use of very small samples coated on a platinum ribbon heater/thermometer mounted in close proximity to the electron beam of a Bendix Time-of-Flight (TOF) mass spectrometer. Heating of the sample by capacitor or battery discharge was synchronized with the TOF analysis cycles. These techniques afford several distinct advantages in the study of thermal decompositions:

o The vacuum essential to operation of the TOF assures identification of the primary decomposition species.

o A very small amount (5-10 micrograms) of sample is applied as a thin coating on a comparatively large mass of supporting ribbon, assuring close compliance of the sample temperature to the ribbon temperature at all times.

o The inclusion of the platinum ribbon in a resistance bridge circuit so that it acts as its own thermometer to eliminate errors in temperature measurement associated with external measuring systems, i.e., emittance values for optical pyrometry, large heat sink and thermal lag of attached thermocouples or other heat-sensing devices.

o Method sensitivity, resolution, wide response range, allows continuous separation and analysis of decomposition species at widely different reaction rates.

---

\* This work was supported by Air Force Contract AF04(611)11385, from Air Force Rocket Propulsion Laboratory, Research and Technology Division, Edwards, California, Air Force Systems Command, United States Air Force.

o The very rapid ( $3 \times 10^7$  °C/sec.) heating rate attainable with the capacitor discharge permits stepwise isothermal analysis of the sample decomposition at the desired pyrolysis temperature. This is essential for determining induction times to explosion, similar to Wenograd's method (Ref. 1). This method is called Isothermal Flash Mass Thermal Analysis (or Isothermal FMTA).

o The less rapid heating rates (10-1000 °C/sec.) attainable over longer times (linear up to 2 sec. at 100 °C/sec.) permit study of reactions which control the stability/shelflife of the material or propellants, as well as of the reactions which occur in the thermal wave zone at the surface of a burning propellant. All quantities measured by this system are mathematically differentials so that many factors may be derived without extensive, tedious, and possibly inapplicable calibration procedures. This method is called Dynamic FMTA.

o Reaction mechanisms can be inferred from the order of appearance and temperature of appearance of the various pyrolysis species.

These techniques were originated in 1962 for the study of the phenomena which occur in the fizz zone of a burning propellant when the temperature rises from that of the bulk of propellant ( $\sim 300$ °K) to that of the flame (up to 3000°K), within a distance of approximately 1 millimeter, creating high temperature and concentration gradients. Subsequently, and with some modification, this technique has provided an equally powerful tool for elucidating the decomposition mechanisms and energetics of high energy binders and oxidizer pyrolyses at heating rates in the range of 100 to 200 °C/sec. Data acquisition, as well as data reduction techniques, have been developed which are necessary to elucidate the detailed decomposition reactions for the primary products under a broad range of experimental conditions (e.g., heating rates). Mathematical models have been developed which have been used in conjunction with a computer to establish the temperature across the sample area on the platinum ribbon heater. A mathematical technique has been developed which takes advantage of the unique differential data acquisition mode during dynamic FMTA to derive reaction activation energies, and eventually, the absolute reaction rates.

### 3. EXPERIMENTAL TECHNIQUES

Thermal decomposition rates of propellants/propellant ingredients can be very high. The instruments and techniques used to study the pyrolysis of these compounds should, therefore, be capable of acquiring data at rates characteristic of the processes. The mass thermal analytical technique developed for such investigations utilizes the fast scan speed of the Bendix TOF mass spectrometer. The sample, weighing 5 to 20 micrograms, is coated on a resistive platinum ribbon which is located 2 millimeters from the ionizing electron beam of the mass spectrometer. The ribbon and sample is heated by means of a battery discharge for slow heating rates or a capacitor discharge for fast heating rates. The ribbon forms one arm of a Wheatstone bridge, by means of which the temperature-time profile of the ribbon and sample is determined. For heating rates in the range of 10 to 1000 °C/sec., the mass spectra displayed on an oscilloscope are monitored continuously by fast cinematography. The experimental arrangement is shown schematically in Figure 1.

a. The Bendix Time-of-Flight Mass Spectrometer (TOF)

The TOF instrument consists basically of three sections: the ionization chamber, the flight tube, and the detector multiplier. In the normal mode of operation, ions are produced by a beam of electrons of controlled energy every 50 to 100 microseconds. (A 100 microsecond cycle can be easily achieved). Immediately after the electron pulse, voltage pulses are applied which accelerate the positive ions with identical kinetic energies per unit charge into the flight tube. Because the flight tube is field-free, the ions travel at velocities proportional to  $\sqrt{e/m}$  ( $e$  and  $m$  are charge and mass, respectively) and thus arrive at the detector at different times. The detector multiplies the signal resulting from each group of ions with given arrival times, yielding an intensity--arrival time ( $m/e$ ) spectrum of the ions produced in the ionization chamber. When the voltage and electron pulses are applied every 100 microseconds, a complete spectrum (in the  $m/e$  range of interest here) is obtained every 100 microseconds.

Mass resolution of the Bendix is such that no more than a 1 percent peak height contribution exists between adjacent peaks (one mass unit apart) in the Hg spectrum at  $m/e$  of 200.

b. The Sample Holder

To achieve high heating rates, it is essential that the sample holder be of low mass (low heat content). Since it is desirable to electrically heat the sample, the geometry must be such as to ensure a reasonable electrical resistance for ohmic heating. The sample holder must also be constructed of a relatively non-reactive metal. All these constraints dictated the use of a platinum ribbon sample holder. The wide, flat ribbon (15 by 1.02 by 0.025 mm) permits distribution of the small sample over a large area, resulting in a very thin film which ensures good thermal contact and close compliance of sample temperature to the ribbon temperature.

A Bendix Direct Inlet Probe, Model 843A, which permits access to the mass spectrometer ionization chamber by means of a pumped vacuum lock, was adapted to support the platinum ribbon which bears the sample. The arrangement is shown in Figure 2. When the probe is positioned in the mass spectrometer, the sample is approximately 2 millimeters from the ionizing electron beam. This arrangement results in a higher intensity spectrum than would be possible for a system in which the sample was located at greater distances from the electron beam. Also, products which are shortlived may be detected before they decay to secondary species.

The ionization chamber is cryogenically pumped with two specially designed liquid nitrogen cold traps. Their function is two-fold; (a) the residual  $H_2O$  background is reduced to practically zero and (b) pyrolysis products which escape from the ionization region are trapped before they can rebound from the walls and reenter the ionization region. This insures that most of the products which are being analyzed are detected while in a high energy state and have not collided with sampling system walls.

### c. Sample Heating System

In these experiments, the sample may be heated in two different modes: (a) flash heating ( $3 \times 10^7$  °C/sec.) to an isothermal condition and (b) a slower temperature rate of increase which has been varied from 100-200 °C/sec. In either case, the platinum filament constitutes one arm of a Wheatstone bridge. Just prior to each sample run, the bridge is nulled. As the ribbon is heated, its resistance changes and the bridge becomes unbalanced. The output signal of the bridge is fed to an oscilloscope and recorded photographically. The circuit diagram is presented in Figure 3.

The heating of the ribbon during Dynamic FMTA is produced by a 24-volt battery connected in series with the bridge. The rate of heating may be varied with a rheostat also in series with the bridge. This is the only method which was used for the work reported herein.

Flash heating of the sample to an isothermal condition for Isothermal FMTA is accomplished by discharging a high voltage from a capacitor through the platinum ribbon. The capacitor is charged by the hydrogen thyratron. A constant low voltage from a 24-volt battery serves as the bridge power supply which enables the temperature to be measured after the current surge from the capacitor has subsided. The duration of the capacitor discharge is less than 10 microseconds. As in the dynamic FMTA, the bridge output is fed to an oscilloscope and is recorded photographically.

In both modes, the resistance of the platinum ribbon is calculated from the well-known Wheatstone bridge relationships, using the bridge imbalance potential at selected time intervals. The temperature at each time is then derived from the known resistance-temperature behavior of the platinum ribbon.

### d. Data Recording Techniques

Time-of-flight mass spectrometry lends itself well to fast pyrolysis studies because of its rapid sampling rate (10 KHz) over the spectrum of 12 to 250 mass units. This rapid rate permits the use of very small samples and small heat sources which characteristically possess low heat capacities and therefore require less energy for a given temperature increase.

Rapid analysis coupled with extremely short periods in which the pyrolysis products are available for detection present some stringent requirements for recording data. In these experiments, the time range of interest may be as short as a hundred microseconds or, at most, two seconds. Obviously, the data must be recorded photographically from an oscilloscope trace.

For the dynamic FMTA, a Milliken DBM-5C high speed framing camera was employed to photograph the spectrum oscilloscope trace at a speed of 200 frames/second or 1 frame each five milliseconds. In general, the nominal heating rate was 100 °C/sec. With the small sample, the pyrolysis event was usually completed within two seconds. To synchronize the temperature trace oscilloscope with the spectrum displayed on the oscilloscope, a flashlamp was triggered simultaneously with the beginning of current input to the ribbon. The flash overexposes the first few frames

of the spectrum, thereby marking the beginning of the heating. The same trigger pulse that fires the flashlamp is also used to trigger the sweep of the temperature trace oscilloscope. Since the mass spectrograph operates continuously at 100 microsecond intervals, the experiment may be begun at any time without an error in time of greater than 100 microseconds. This presents no serious error in time or temperature for experiments lasting one second; covering 10,000 complete spectra. The mass spectra, from  $m/e = 12$  to  $m/e = 250$  are continuously displayed on another oscilloscope. This trace is photographed by a camera operating at 200 frames per second, so that data is recorded at five millisecond intervals. This is sufficiently fast to permit accurately following the species formed in reactions induced by heating at rates from 100 to 200°C/sec. In this heating rate range, the rate of temperature rise is 0.1 to 0.2°C/millisecond, which corresponds to 0.01 to 0.02°C/complete mass spectrum trace or to 0.5 to 1.0°C/frame of film. Therefore, errors in temperature correlation, induced by one or several frame uncertainty for the start of the experiment would introduce an error no greater than that involved in the initial (zero time) sample temperature measurement.

#### e. Sample Preparation

A critical step in this analysis technique is insuring that the sample is uniformly distributed over the surface of the pyrolyzing heat source. From the standpoint of heat transfer to the sample source heat capacity and low pressure requirement of the mass spectrometer vacuum the sample must be on the order of 5-20 micrograms to achieve the best results. Samples of solid oxidizers or fuels have been dissolved in suitable solvents and deposited on the center 0.5 centimeter of the platinum ribbon in a dry box. For example,  $HP_2$  is applied to the surface as a uniform film of a known concentration in dry methyl alcohol by means of a micro syringe, and the solvent allowed to evaporate. The sample is then transferred, in a dry bag, to either the mass spectrometer or to a bell jar and subjected to vacuum for 2 to 20 hours to remove the last traces of solvent. The sample, on the ribbon and holder, is then affixed to a probe, inserted into position inside the mass spectrometer through the vacuum lock. The sample is then heated by the battery discharge for dynamic FMTA.

### 4. DATA REDUCTION AND ANALYSIS

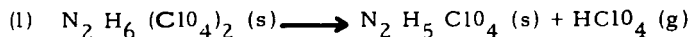
#### a. Hydrazinium Diperchlorate ( $HP_2$ ) Decomposition

The technique has been termed Dynamic Flash Mass Thermal Analysis (or Dynamic FMTA, for short). This terminology arises by analogy to thermal methods of analysis already in use, especially thermogravimetric analysis (TGA) techniques which it most closely resembles. There are two basic modes of operation. The first mode utilizes linearly programmed heating combined with continuous analysis by the mass spectrometer, and thus is analogous to dynamic TGA. The second mode uses an extremely fast heating to an isothermal condition, and thus resembles isothermal TGA. Since the heating rates in either mode are extremely rapid compared to those in common use, the heating mode is analogous to "flash" heating by other means. Therefore, the first and second modes are aptly described as Dynamic FMTA, and Isothermal FMTA, respectively. The dynamic FMTA method has been used to study the decomposition mechanisms and energetics of  $HP_2$  and NC, and to establish the validity of the technique.

This method also closely resembles the Differential Thermal Analysis (DTA) or Differential Scanning Calorimetry (DSC) techniques as regards linearly programmed sample heating rates and data evaluation, except that the data represent analytical time resolved mass spectra data instead of integrated caloric/thermal data, and a considerably faster instrument response time is provided by using high speed cinematography of the scope display rather than recorders (as in DTA).

The films taken of the mass spectral traces are analyzed frame-by-frame for the order of appearance of species, and the parent species deduced from structural considerations and comparison with standard mass spectra (when available). Figure 4 shows a typical sequence for  $\text{HP}_2$ .

It is expected that the key species in the initiation reaction(s) for thermal decomposition can be those which are attached to the molecule with the weakest bonds, and hence appear first (at low temperatures) in the films of the mass spectra. Several of the key species are selected, and their spectral intensities are plotted as a function of time (and/or temperature), as in Figure 5, to facilitate deduction of the pyrolysis mechanism. The data are consistent with the mechanisms postulated by Grelecki and Cruice (Ref. 2) and by Levy, Von Elbe, Friedman, Wallin and Adams (Ref. 3):



The first peak in the time/intensity plot is definitely due only to  $\text{HClO}_4$ , corresponding to equation (1), whereas the second peak has definite contributions from both  $\text{N}_2\text{H}_4$  and  $\text{HClO}_4$ .

To be able to extrapolate the data obtained at one temperature and reaction rate to another temperature, e. g., shelflife prediction, combustion rates, etc., it is necessary to derive the activation energies and preexponential factors for the reactions. Fortunately, for the determination of the activation energy (E), absolute reaction rate data are not required, but only the shape of the curve and the slope which can be derived therefrom. In the uncalibrated mass spectrometer, the line intensity, I, of a given species is related to its partial pressure, P, in the ion chamber in an unknown but constant proportion during any particular experiment. P, in turn, is proportional to the difference between the rate of generation of a species and the rate at which it is removed by pumping and by injection into the flight tube as ions. The difference is also an unknown but constant factor during any given experiment.

Method I

If the rate of generation of a species can be represented by the Arrhenius rate expression as a first order reaction, then:

$$I \propto P \propto (1/x) (dx/dt) = k = A \exp. (-E/RT)$$

or

$$I = B \exp. (-E/RT)$$

Wherein B contains the Arrhenius frequency factor, A, the mass spectrometer system constants, and the fraction, x, of a given species which remains unreactive at any given time. Consideration of x as constant over a small time or temperature interval introduces only a small error in calculating E, since it is the fraction reacted which is important in this case, and not the absolute quantity. Taking the logarithm of the function yields:

$$2.303 \log I = -E/RT + 2.303 \log B$$

A plot of  $\log I$  versus  $1/T$  should yield a straight line with a slope of  $-E/(2.303R)$ . The intercept at  $\log I = 0$  will yield a value of  $\log B$  which may be of value later to evaluate A, specific reaction rates, and mass spectrometer system constants.

Method II

For complete definition of the reaction kinetics, the value of the reaction rate, reaction rate constant, or pre-exponential factor must be determined as well as the activation energy. The rate of disappearance of reactant, hence rate of appearance of products, during a first order reaction is given by:

$$dx/dt = kx$$

or:

$$(1/x)(dx/dt) = k$$

which is mathematically identical to:

$$d(\ln x)/dt = k \text{ (where } \ln \text{ refers to natural logarithms)}$$

on integration between limits:

$$\ln x_2 - \ln x_1 = \ln (x_2/x_1) = k (t_2 - t_1)$$

Since the ratio  $x_2/x_1$  is the same whether  $x$  is an absolute value or a fraction of the absolute value, the above rate expressions are likewise indifferent to the way in which  $x$  is expressed. This fact, together with the differential nature of the analytical technique provides the key whereby the absolute reaction rates and pre-exponential factors may be derived from the data taken by the uncalibrated system. The total area enclosed by the intensity/time curve for a given mass species represents the total quantity of that species which was formed as the result of the reaction. Any portion of the total area, taken at a definite time, then represents a definite fraction of the quantity of that species which has been formed. The total area, and suitable fractions thereof, taken at short time intervals during the initial stages of the reaction, can be replotted as  $\ln x$  versus time. Since each time corresponds to a definite temperature, the slopes of the plot, taken at several times, correspond to values of the absolute reaction rate constant,  $k$ , taken at several temperatures. The  $\ln k$  can then be plotted against reciprocal absolute temperature in the conventional manner, and both the activation energy and the pre-exponential factor,  $A$ , determined routinely.

It is expected that the activation energy for the thermal decomposition reaction of a compound will reflect the activation energy of the primary decomposition species. Therefore, the Arrhenius plots of the first detected species in the  $HP_2$  decomposition calculated by Method I are presented in Figure 6. There are two distinct regimes - the first, "low temperature" regime (labeled "A" on the graphs) is driven solely by the energy input from the platinum ribbon, while the second, "high temperature" regime (labeled "B" on the graphs) is one in which autoacceleration of the reaction occurs.

Work on  $HP_2$  was performed at Thiokol's Reaction Motors Division (RMD) (Ref. 2), using time-to-acceleration techniques with a closed vessel. This technique yields the activation energy for a reaction which occurs before autoacceleration - which corresponds to the "A" regime. The data as presented in Figure 6 for the "A" regime yields a value of 23 Kcal/mole, which compares remarkably well with the value of 23.5 Kcal/mole obtained at RMD. Thus, the validity of the experimental and data reduction techniques is established. The activation energy and frequency factor determined from the more detailed data treatment of Method II are given in Table I. It should be noted that the activation energy is determined from the first  $\frac{1}{2}\%$  decomposition, and very small errors in the determination of the fractional areas will yield large errors in the value of the activation energy. Other large errors can be introduced when small errors are made in selecting the slopes from the curves of fraction reacted versus time (from which the reaction rate constant,  $k$ , is obtained). The slopes are very sensitive to the way in which the curves are drawn, and to personal judgment in estimating the tangent line. Under these circumstances, the agreement of the two sets of data is encouraging. Future determinations will be made with much more care over the first one to two percent of the decomposition in order to improve the accuracy of the results.

When the activation energy of 23 Kcal/mole is used with the absolute rate constants obtained in the detailed treatment, the Arrhenius factor is found to be  $(5 \pm 2) \times 10^{13} \text{ sec.}^{-1}$ , which is a reasonable value for these types of reactions.

It is of interest to note that the vacuum conditions prevailing in these experiments precludes the acceleration of the reaction by reaction products, so that another explanation for the observed acceleration must be sought. The experimental results show that the activation energy for the initial step changes from 23 Kcal per mole during the pre-acceleratory period to 86 Kcal per mole during acceleration. This means that the acceleration of the reaction (rate of change in reaction rate due to one degree centigrade temperature rise) is more than 12 times as great for the portion with the 86 Kcal/mole activation energy as for the portion with the 23 Kcal/mole activation energy.

#### b. Hydrazinium Monoperchlorate (HP) Sublimation

The postulated decomposition mechanism, chemical equations (1) and (2) suggests the possibility of also obtaining the heat of sublimation of HP from the FMTA data. Since  $N_2H_4$  is characteristic of HP only, then the heat of sublimation should be found by applying the Clausius-Clapeyron equation to the  $m/e = 23$  ion species ( $N_2H_3^+$ ). The previous arguments regarding mass spectrometer system constants apply to this determination as well. The integrated form of the Clausius-Clapeyron equation is:

$$-\ln I \propto -\ln P = \left( \frac{\Delta H_{\text{sub.}}}{R} \right) \left( \frac{1}{T} \right) + \text{constant}$$

As before, the pressure ratios are equivalent to the intensity ratios, so that a plot of  $\ln I$  versus  $1/T$  will yield a straight line with slope equal to  $-\Delta H_{\text{sub.}}/R$ . From this plot, shown in Figure 7, the heat of sublimation,  $\Delta H_{\text{sub.}}$ , is calculated to be 32 Kcal/mole. This compares very well with the value of 29.2 Kcal/mole determined by Levy et alii (Ref. 3), using an equilibrium vacuum sublimation technique.

## 5. CONCLUSIONS

The FMTA technique has been shown to be a powerful tool for the investigation of thermal decomposition of solid materials since the reaction mechanisms and kinetic rate data can be obtained from a single experiment. In some cases, kinetic data (e.g., Arrhenius frequency factors) and primary decomposition species can be obtained by no other current technique. The results of the FMTA technique do not depend upon tedious, unreliable, and repeated mass spectrometric calibration procedures, therefore many more useful experiments can be performed with equipment previously considered unsuitable for quantitative measurements.

## BIBLIOGRAPHY

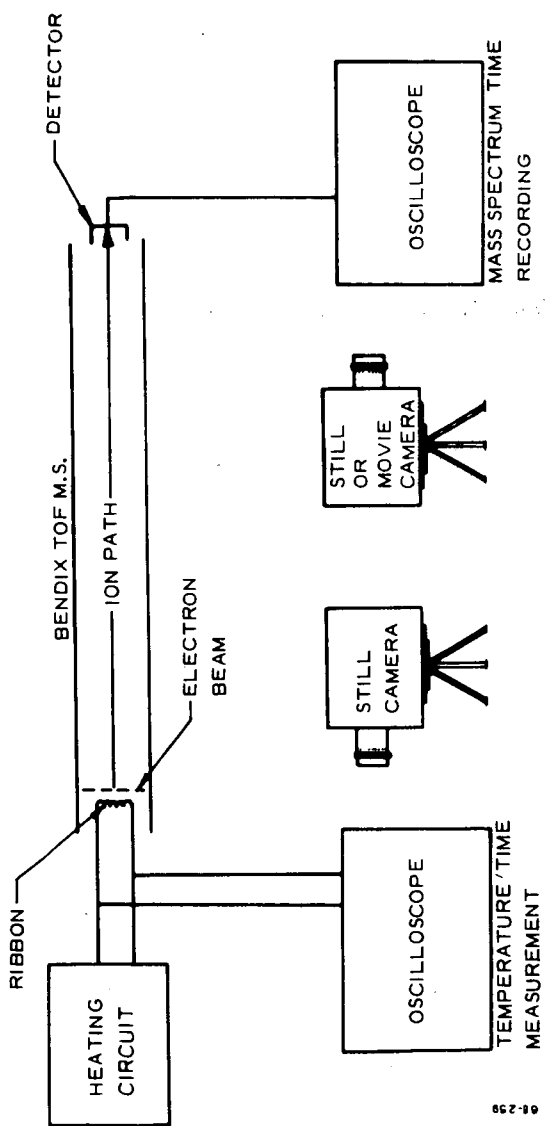
1. J. Wenograd, "The Behavior of Explosives at Very High Temperatures", U.S. NOL, NAVWEPS Report 7328, Oct. 1960
2. C. J. Grelecki, W. Cruice, "Thermal Decomposition of Hydrazinium Monoperchlorate and Hydrazinium Diperchlorate", pp 73-81, in *Advanced Propellant Chemistry, Advances in Chemistry Series 54*, American Chemistry Society, Washington, D. C. (1966)
3. J. B. Levy, G. Von Elbe, R. Friedman, T. Wallin, S. J. Adams, "The Deflagration of Hydrazine Perchlorate", pp 55-72, *ibid.*

TABLE I  
ENERGIES FOR HP<sub>2</sub> THERMAL EVENTS

<u>Species</u>	<u>m/e</u>	Decomposition Activation Energies (Kcal/mole)		
		<u>This Work</u>		<u>(Ref. 2)</u>
		<u>A</u>	<u>B</u>	
HClO <sub>4</sub> <sup>+</sup> (parent)	100	23	86	23.5

HP HEAT OF SUBLIMATION (Kcal/mole)

<u>Species</u>	<u>This Work</u>	<u>(Ref. 3)</u>
N <sub>2</sub> H <sub>3</sub> <sup>+</sup> (from N <sub>2</sub> H <sub>4</sub> )	32	29.2



9-23

Figure 1 MTA Experiment Schematic

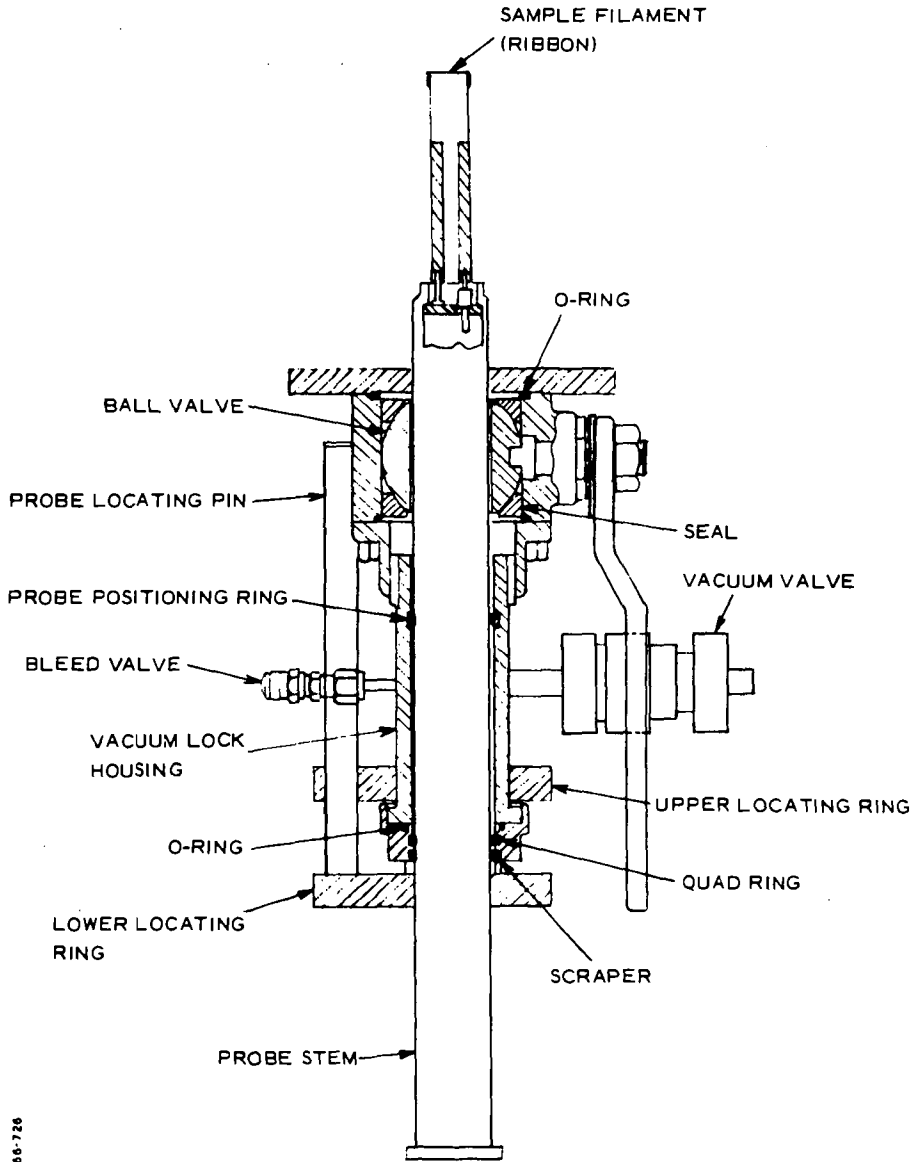


Figure 2 Bendix Direct Inlet Sample Probe

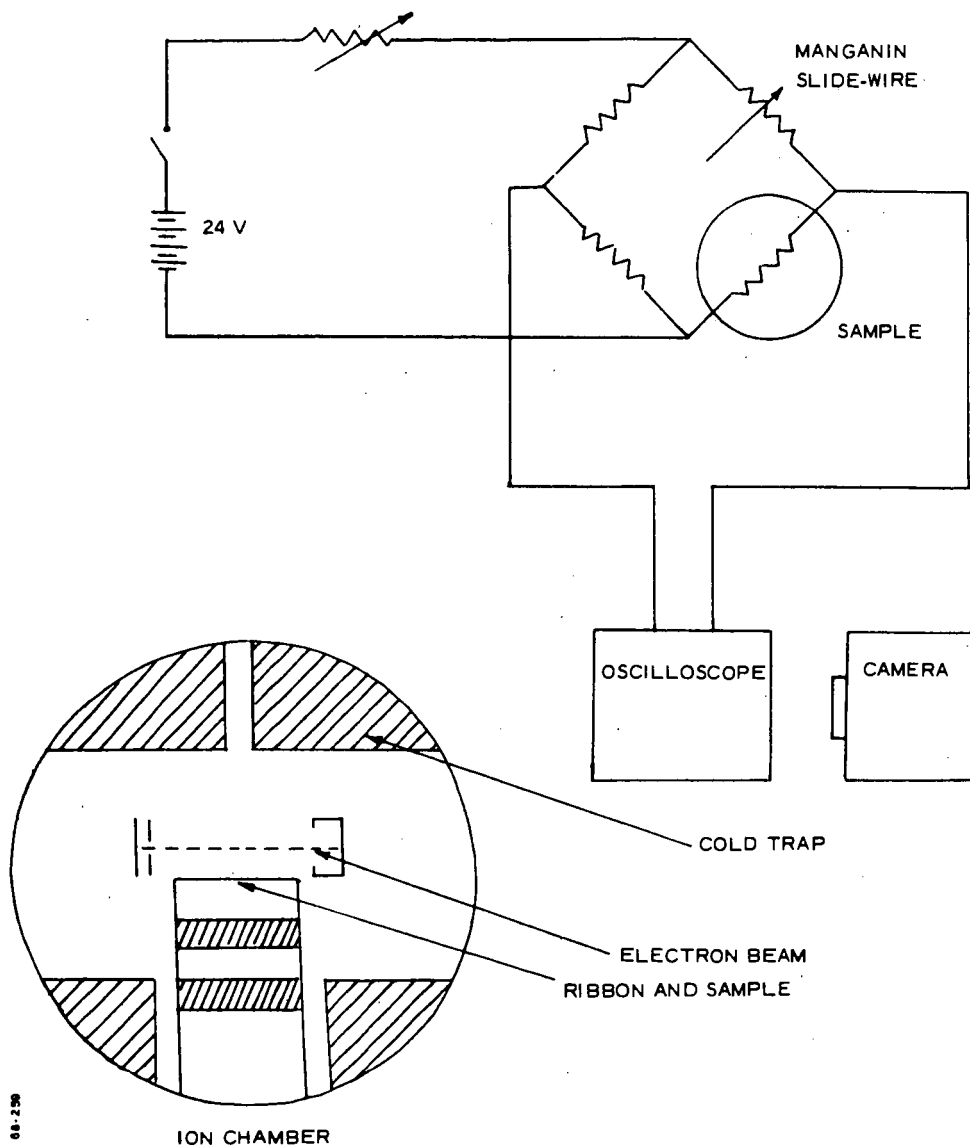


Figure 3 Dynamic FMTA Schematic

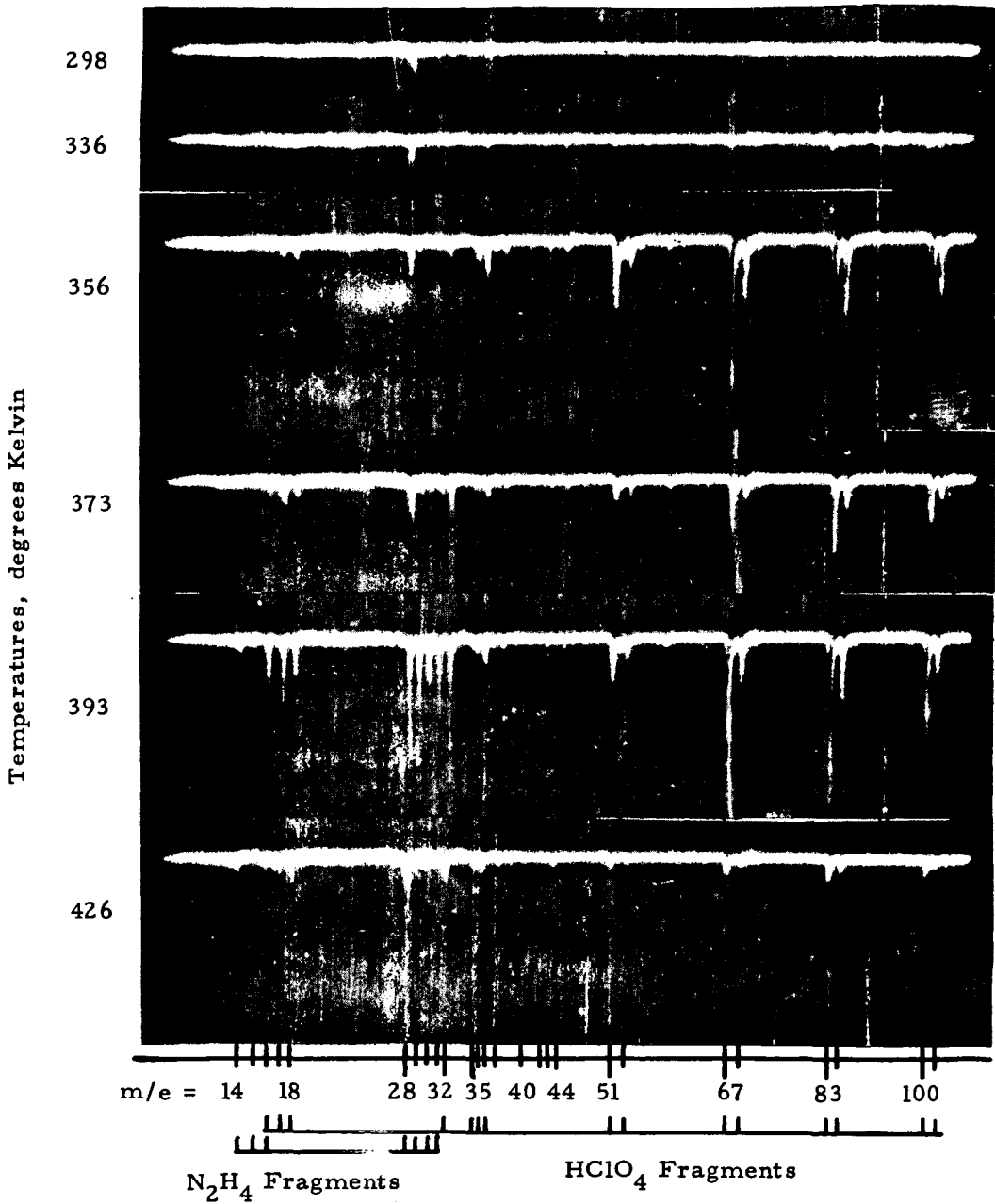


Figure 4 Mass Spectra from FMTA of  $HP_2$

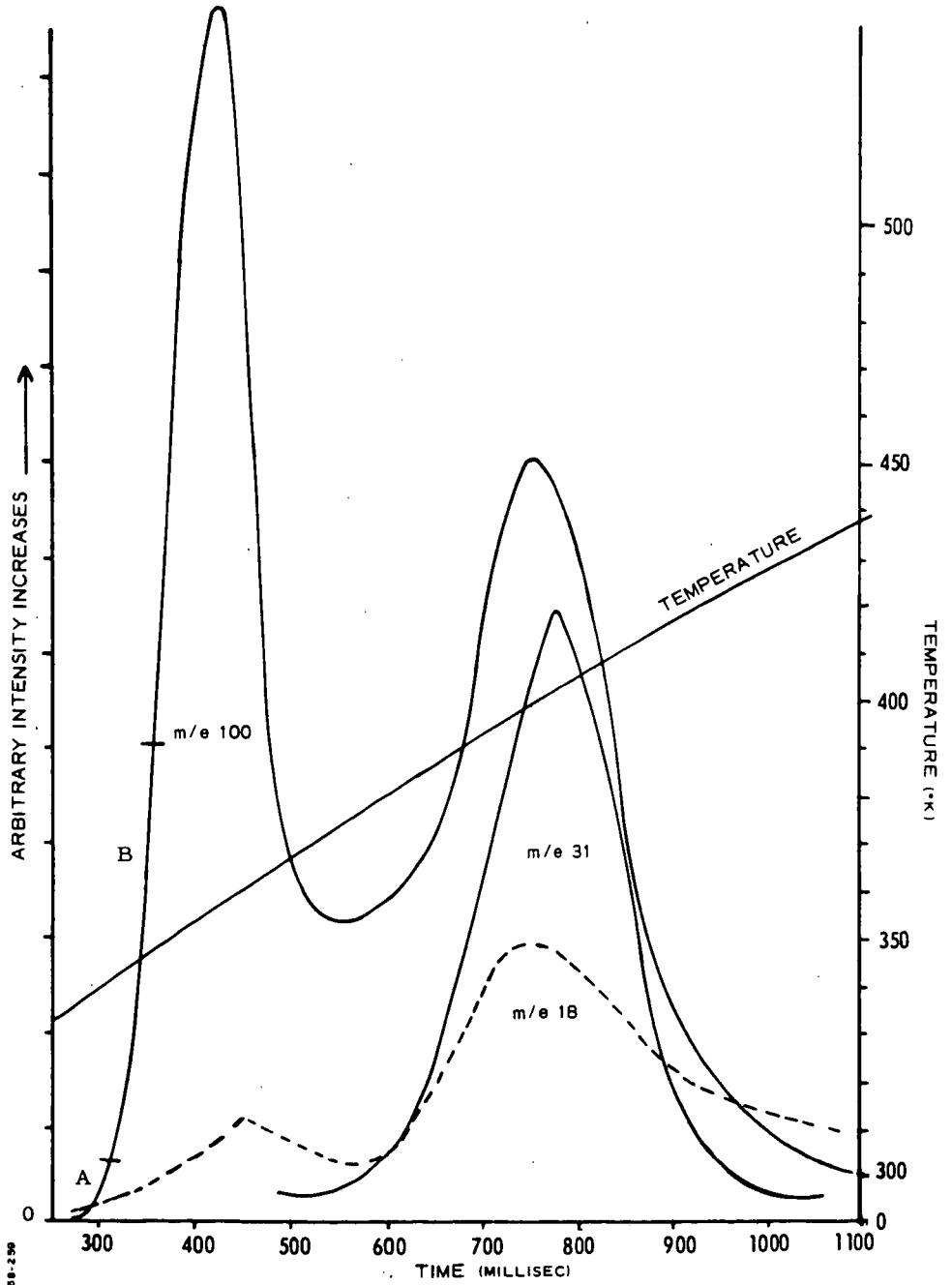


Figure 5  $HP_2$  Pyrolysis Fragment Histories

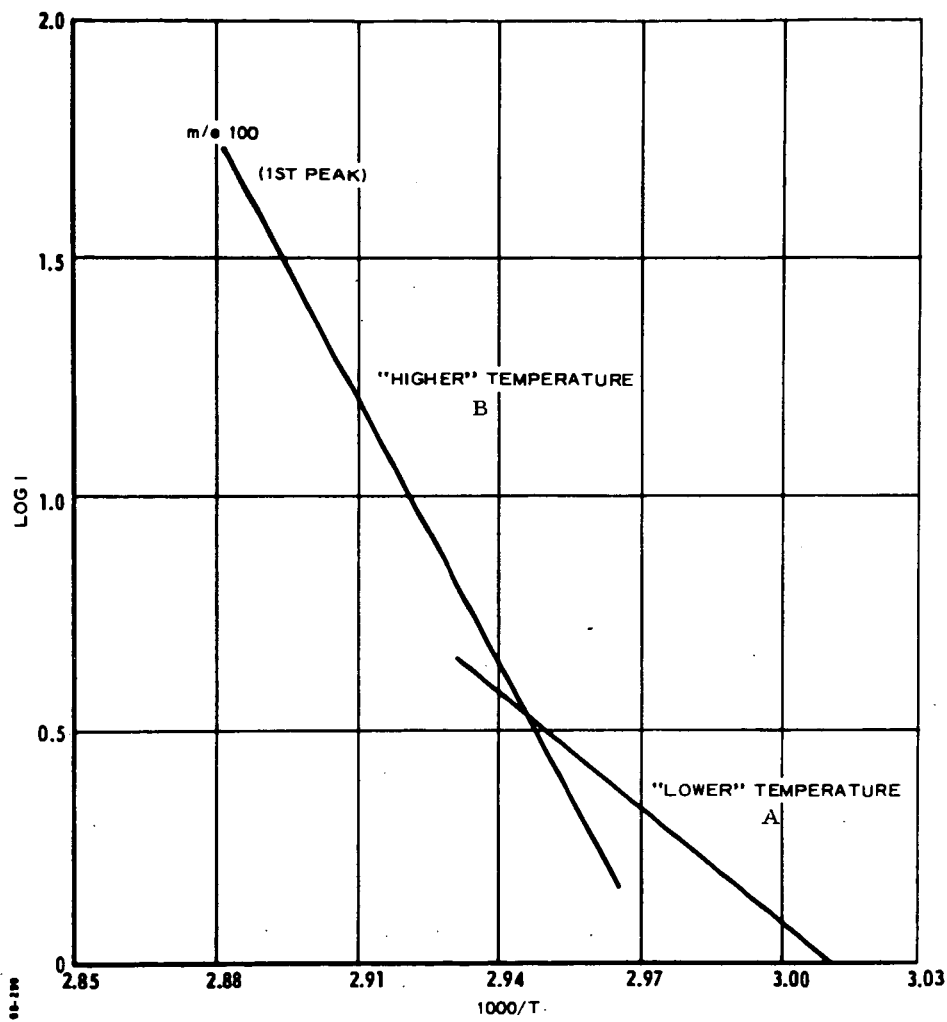


Figure 6 Arrhenius Plot of  $\text{HClO}_4^+$  from Flash MTA of  $\text{HP}_2$

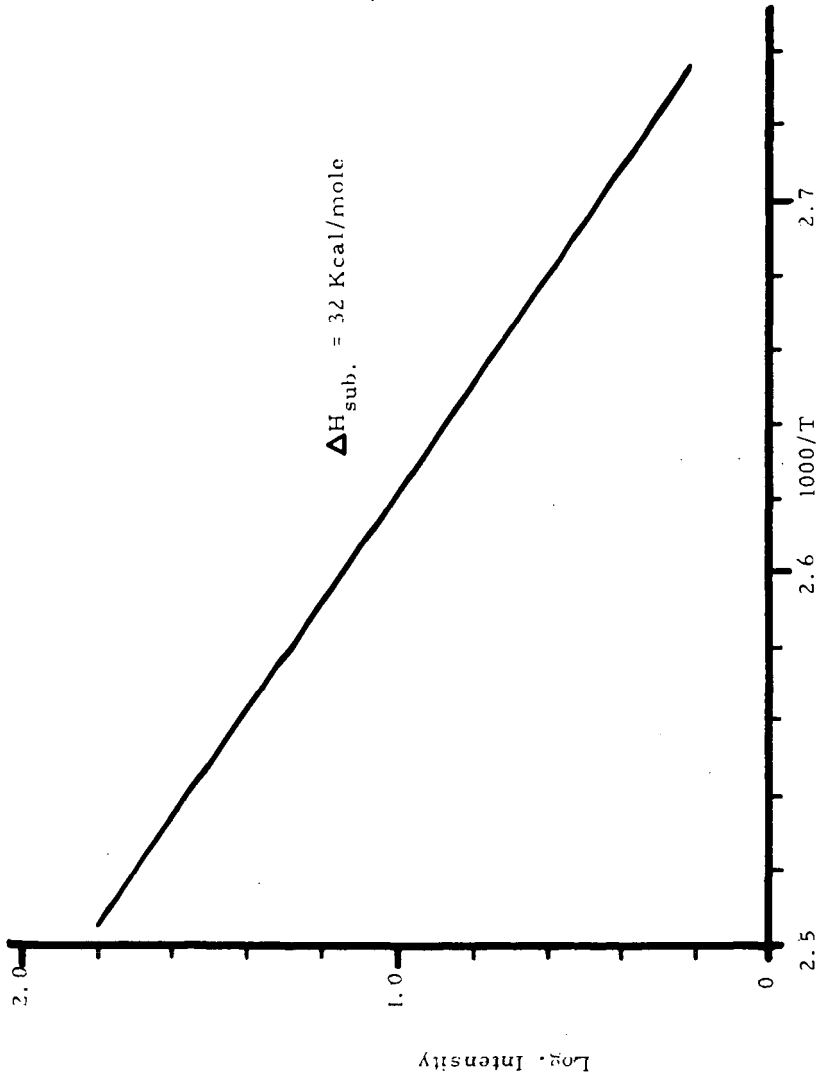


Figure 7 Clausius-Clapeyron Plot for HP Sublimation